Chemical Geology 251 (2008) 99–111

Contents lists available at ScienceDirect

Chemical Geology

journal homepage: www.elsevier.com/locate/chemgeo

Geochemistry of apatite-rich layers in the Finero phlogopite–peridotite massif (Italian Western Alps) and ion microprobe dating of apatite

Tomoaki Morishita [a,b,c,*], Kéiko H. Hattori [d], Kentaro Terada [e], Takuya Matsumoto [f,1], Koshi Yamamoto [g], Masamichi Takebe [g,2], Yoshito Ishida [a], Akihiro Tamura [a], Shoji Arai [a,h]

[a] Frontier Science Organization, Kanazawa University, Kakuma, Kanazawa 920-1192, Japan
[b] CNR-Instituto di Geoscienze e Georisorse Sezione di Pavia, via Ferrata 1, I-27100, Pavia, Italy
[c] Frontier Science Organization, Kanazawa University, Kakuma, Kanazawa 920-1192, Japan
[d] Department of Earth Sciences, University of Ottawa, Ottawa, Canada K1N 6N5
[e] Department of Earth and Planetary Science, Hiroshima University, Kagamiyama 1-3, Higashi-Hiroshima, 739, Japan
[f] Graduate School of Science, Osaka University, Machikaneyama, Toyonaka, Osaka 560-0043, Japan
[g] Department of Earth and Planetary Sciences, Graduate School of Environmetal Studies, Nagoya University, Nagoya, Aichi 464-8602, Japan
[h] Institute for Research on Earth Evolution, Japan Agency for Marine-Earth Science and Technology, Yokosuka, Kanagawa 237-0061, Japan

ARTICLE INFO

Article history:
Received 17 July 2007
Received in revised form 20 February 2008
Accepted 28 February 2008

Editor: R.L. Rudnick

Keywords:
Finero peridotite
Metasomatism
Apatite
Carbonate

ABSTRACT

Highly metasomatized apatite-rich peridotite layers (AP-layer) occur in the Finero phlogopite–peridotite massif (western Italian Alps). The AP-layer and the host peridotite are characterized by higher concentration of REE (total REE > 80ppm), especially LILE, and lower HFSE, than those of the other rocks in the Finero massif. The AP-layers and their host peridotites have bulk silicate Earth-like Sr and Nd-isotope compositions except for one sample containing rare carbonate aggregates. The carbonate aggregates occur in a late serpentine-talc veinlet and show relatively high $d^{13}C$ and $d^{18}O$, high $^{87}Sr/^{86}Sr$ and lower εNd than the other samples. These results, combined with the previous data, indicate that the carbonates formed late at relatively low temperatures. The petrochemical results along with the literature suggest that the AP-layer was locally formed from a metasomatic agent geochemically distinct from that formerly producing phlogopite-bearing harzburgite widely distributed throughout the massif. We propose that the metasomatic agent for the AP-layer was an orthopyroxene-saturated, CO_2-bearing hydrous fluid/melt that evolved through the crystallization of metasomatic minerals upon reactions with peridotites. Sensitive high-resolution ion microprobe (SHRIMP) analyses of apatite grains yielded a Tera-Wasserburg concordia three-dimensional isochron age of 215 ± 35Ma in the $^{238}U/^{206}Pb$–$^{207}Pb/^{206}Pb$–$^{204}Pb/^{207}Pb$ diagram. The age is similar to intrusions in the Finero area, suggesting that the carbonate- and apatite-metasomatism was synchronous with Triassic magmatic activity.

1. Introduction

Mantle metasomatism is caused by the infiltration of metasomatic fluids or melts in diverse tectonic settings under a wide range of *P–T* conditions (e.g., Zinngrebe and Foley 1995; Vannucci et al., 1998; Wulff-Pedersen et al., 1999; Arai et al., 2003; Morishita et al., 2003a; Arai et al., 2004). Apatite in mantle xenoliths has been reported from intraplate or continental rift settings (e.g., Griffin et al., 1988; O'Reilly and Griffin, 1988; Yaxley et al., 1991; Hauri et al., 1993; Rudnick et al., 1993; Ionov et al., 1996; Bedini and Bodinier, 1999; Kaliwoda et al., 2007; Kaeser et al., 2007), mantle wedges (e.g., McInnes and Cameron, 1994; Laurora et al., 2001; Demény et al., 2004) and backarc lithosphere (Rivalenti et al., 2004). Apatite contains high concentrations of rare earth elements (REE), Cl, F, U, Th, Sr and hence, plays an important role in the behavior of these elements in the upper mantle (e.g., Watson, 1980; Exley and Smith, 1982; Griffin et al., 1988; O'Reilly and Griffin, 1988, 2000; Ionov et al., 2006). The study of the formation of mantle-derived apatite helps in understanding not only the metasomatic processes that locally modify the mantle compositions but also the behaviour of incompatible elements in the upper mantle.

The Finero phlogopite–peridotite massif in the western Italian Alps is well known as a highly metasomatized peridotite massif, which has abundant metasomatic minerals, particularly phlogopite and amphibole (Exley and Smith, 1982; Cumming et al., 1987; Voshage et al., 1987; Hartmann & Wedepohl, 1993; Zanetti et al., 1999; Grieco et al., 2001, 2004; Prouteau et al., 2001; Morishita et al., 2003b; Zaccarini et al., 2004; Raffone et al., 2006). The apatite- and carbonate-bearing rocks in the Finero massif were first documented by Zanetti et al.

* Corresponding author. Frontier Science Organization, Kanazawa University, Kakuma, Kanazawa 920-1192, Japan. Tel.: +81 76 264 6513; fax: +81 76 264 6545.
E-mail address: moripta@kenroku.kanazawa-u.ac.jp (T. Morishita).
[1] Present address: Institute for study of the Earth's Interior, Okayama University, Misasa, Tottori 682-0193, Japan.
[2] Present address: Matsue National College of Technology, Matsue, Shimane 690-8518, Japan.

0009-2541/$ – see front matter © 2008 Elsevier B.V. All rights reserved.
doi:10.1016/j.chemgeo.2008.02.018

(1999) around the pyroxenite layers (wehrlite in modal compositions) whereas Morishita et al. (2003b) further reported an apatite-rich peridotite layer (AP-layer) from this area. The origin of the metasomatic agent and nature of metasomatic processes that operated in the Finero massif are still in debate. This paper presents the compositions and isotope data of whole-rock samples and metasomatic minerals, as well as the in-situ U–Pb ages of apatite in order to discuss the evolution of the metasomatic agent responsible for the formation of the AP-layer in the Finero massif.

2. Geological background

The Finero mafic–ultramafic complex represents the northwestern basal portion of the Ivrea zone, a slice of lower crustal rocks of the African plate accreted onto the European plate during the Alpine orogenesis (Nicolas et al., 1990), at the western end of the Southern-Alpine domain. The entire complex has been folded into a tight antiform and divided into four main units: (1) upper metagabbro, (2) amphibole–peridotite, (3) lower metagabbro, and (4) phlogopite–peridotite (Lensch, 1968; Hunziker, 1974; Cawthorn, 1975; Coltorti and Siena, 1984; Siena and Coltorti, 1989; Voshage et al., 1987; Hartmann and Wedepohl, 1993). The phlogopite–peridotite unit (unit 4) consists of dunite and harzburgite with minor clinopyroxenites and chromitites. Platinum-group minerals, zircon, zirconolite and Zr–Th–U minerals were reported from chromitites by Ferrario and Garuti (1990), Grieco et al. (2001, 2004), and Zaccarini et al. (2004).

Previously reported ages of the massif include zircon ages of the chromitites, 204–208 Ma (Von Quadt et al., 1993, Grieco et al., 2001) and K–Ar ages of phlogopite and amphiboles, 206 ± 9Ma and 1290 ± 75Ma, respectively (Hunziker, 1974): the latter unrealistic old age of amphibole was explained by excess ^{40}Ar in the sample. Hunziker (1974) also obtained a ^{40}K–^{40}Ar isochron age of 180 Ma from the phlogopite and amphibole samples. Hartmann and Wedepohl (1993) obtained Rb–Sr ages varying from 226 to 163Ma based on four amphibole–phlogopite pairs. They also cited a ^{39}Ar/^{40}Ar plateau age of 220 ± 3Ma for phlogopite from the unpublished data of V. H. Friedrichsen.

Peressini et al. (2007) summarized the available geochronological data from the Ivrea–Verbano Zone. Magmatic and/or thermal activities at around 220 Ma were extensively documented in and around the Finero complex (Peressini et al., 2007 and references therein). Stähle et al. (1990, 2001) reported alkaline dykes (carbonate-bearing hornblendites and zircon-bearing syenite pegmatite) of Triassic age (220–225Ma). They interpreted that the alkaline magmatism was originated by the partial melting of a metasomatized peridotite of upwelling asthenosphere, whereas Vavra et al. (1999) suggested that these dykes crystallized from alkaline fluids. Oppizzi and Schaltegger (1999) reported a U–Pb zircon age of 212.5 ± 0.5Ma from a plagioclase lens in a layered gabbro near the Finero peridotite massif and interpreted it as a result of the thermal/hydrothermal activity in the lower and middle crustal levels. Voshage et al. (1987) reported a Sm–Nd whole-rock age of 270 ± 57Ma for phlogopite-free peridotite (amphibole–peridotite and also gabbro) in the Finero. Lu et al. (1997) reported a Sm–Nd mineral isochron age of 230 and 210 Ma from the Internal Gabbro Unit in the Finero Complex and interpreted this as a result of a regional heating event. On the contrary, Boriani and Villa (1997) inferred the age as an alteration age.

Triassic geodynamic setting in the Southern Alps including the Ivrea Zone is still in debate (Castellarin et al., 1988; Stähle et al., 2001). On the basis of the correlation of radiometric thermal history with microstructures of the metamorphic rocks, Handy and Zingg (1991) suggested that the extension (crustal rifting) event might have occurred at around Middle Triassic to Early Jurassic stage. The alkaline Triassic magmatic event documented by Stähle et al. (1990, 2001) also supports a rifting event. On the other hand, Castellarin et al. (1988) reported that Triassic magmas with orogenic character are present in

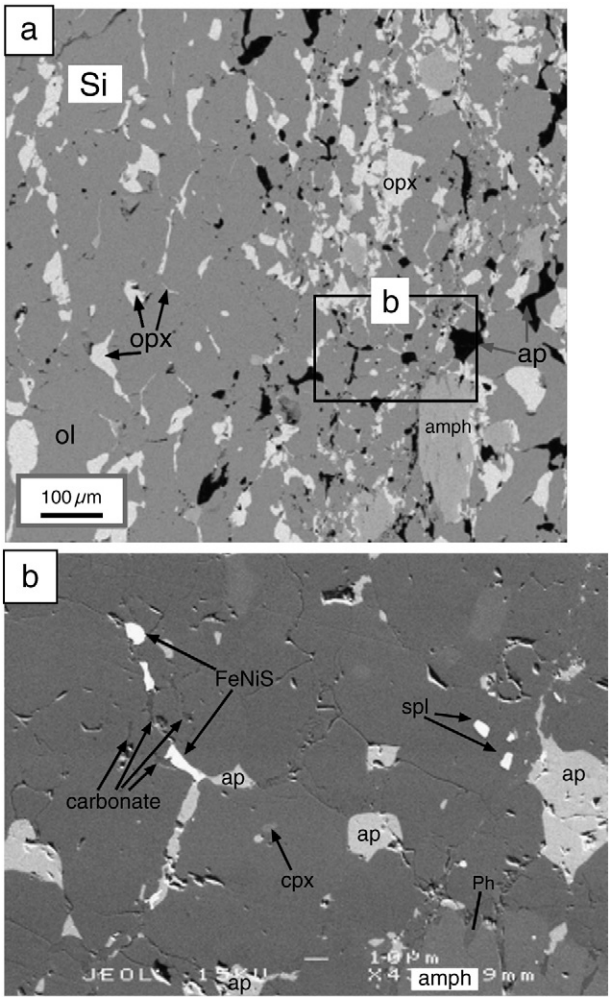

Fig. 2. Microtexture of apatite-rich layer. (a) X-ray intensity maps in Si of the thin apatite-rich layer showing inhomogeneous distributions of apatite and amphibole in the thin layer. Note that apatite and amphibole are more abundant in the right hand than in the left hand. (b) Back-scattered electron image of a part of (a) showing occurrences of minor minerals. Note that carbonate minerals are locally distributed in the sample. amph = amphibole, ap = apatite, cpx = clinopyroxene, FeNiS = Fe-Ni-sulfide, ol = olivine, opx = orthopyroxene, phl = phlogopite, spl = spinel.

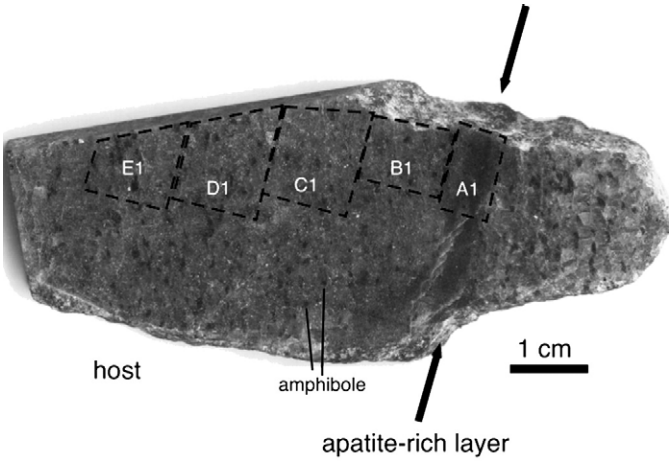

Fig. 1. Sawed surface of the studied phlogopite–peridotite with an apatite-rich layer. Boxes with label show samples which were analyzed for both major- and trace-element compositions.

the Southern Alps. These coupled with the compressional tectonic structures recognized in the eastern part of the Southern Alps (Pisa et al., 1980; Doglioni, 1987) favor a subduction setting rather than a rifting model (Castellarin et al., 1980, 1988; Pisa et al., 1980).

3. Sample description

A large boulder of amphibole-rich harzburgite, 0.8m × 0.4m × 0.3m in size, was collected from the Cannobino river at the Finero village (GPS coordinate: 46°06′15.3″N, 8°37′03.7″E) The harzburgite contains disseminated grains of phlogopite in association with coarse (~ 2 mm) amphibole (Fig. 1). It also contains several AP-layers (< 1 cm in width) that consist of fine-grained (< 100 μm in most cases) olivine, orthopyroxene, spinel, amphibole, apatite, sulfide minerals with minor phlogopite, carbonate and clinopyroxene (Fig. 2). Each AP-layer is divided into apatite-rich part (up to 10 modal% apatite) and volumetrically major apatite-poor part (< 1 modal% apatite) (Fig. 2). The apatite-rich part contains abundant amphibole and carbonate minerals (Fig. 2a). Apatite (10–100 μm in size) is Cl-rich (> 2wt.%; Morishita et al., 2003b). The AP-layer is also characterized by the presence of olivine grains rimmed by orthopyroxene (< 10 μm wide) (Fig. 2a). The orthopyroxene contains small amounts of Al_2O_3 (< 0.2wt.%), Cr_2O_3 (< 0.05wt.%) and CaO (< 0.2wt.%) (Morishita et al., 2003b). Apatite and carbonate also rarely appear in the host harzburgite adjacent to the AP-layer.

Two types of carbonates are recognized. The first type is fine-grained (usually < 10 μm in size) dolomite closely associated with apatite along the grain boundaries of olivine in AP-layers (Fig. 2b; Morishita et al., 2003b). The second type rarely occurs as carbonate aggregates (> 100 μm in size) associated with Mg-poor olivine (Fo = 86) in late serpentine-talc veinlets that cut both the AP-layer and its host rock (Fig. 3).

Clinopyroxene, < 10 μm in size, is rare (less than 1 modal%) in the AP-layer (Fig. 2b). Two types of phlogopites (K-phlogopite and Na-phlogopite) are present in the AP-layer. K-phlogopite (1wt.% Na_2O) is commonly associated with amphibole, whereas rare Na-phlogopite (5wt.% Na_2O) is present in the apatite-rich part of the AP-layer.

4. Chemical compositions

4.1. Analytical methods

For the analyses of whole-rock major- and trace-element compositions, the rock sample containing an AP-layer was cut into ~ 1 cm thick slices perpendicular to the AP-layer, and the slab was further divided into ~ 1 cm wide parallel to the AP-rich layer. A sample, ~ 1 cm × ~ 1 cm × 1 cm, containing the AP-layer in the first slice was named A1, whereas the other pieces of the country rock were named B1, C1, D1 and E1 (Fig. 1). The whole-rock major-element compositions (Table 1) were determined on fused disks with an X-ray fluorescence spectrometer (Shimadzu SXF-1200 with a Rh anode tube) at Nagoya University following the method of Yamamoto and Morishita (1997) and Takebe and Yamamoto (2003). For calibration, JA-, JB- and JP-series reference rock samples distributed from the Geological Survey of Japan (GSJ) were used following the method of Sugisaki et al. (1977). Analytical precision was estimated to be < 1% for SiO_2, < 3% for TiO_2 at the level of < 0.1 wt.% and 3% for other elements. Accuracy was < 5% based on the repeated analyses of selected reference rock standards distributed by the GSJ (Appendix). The whole-rock trace-element concentrations

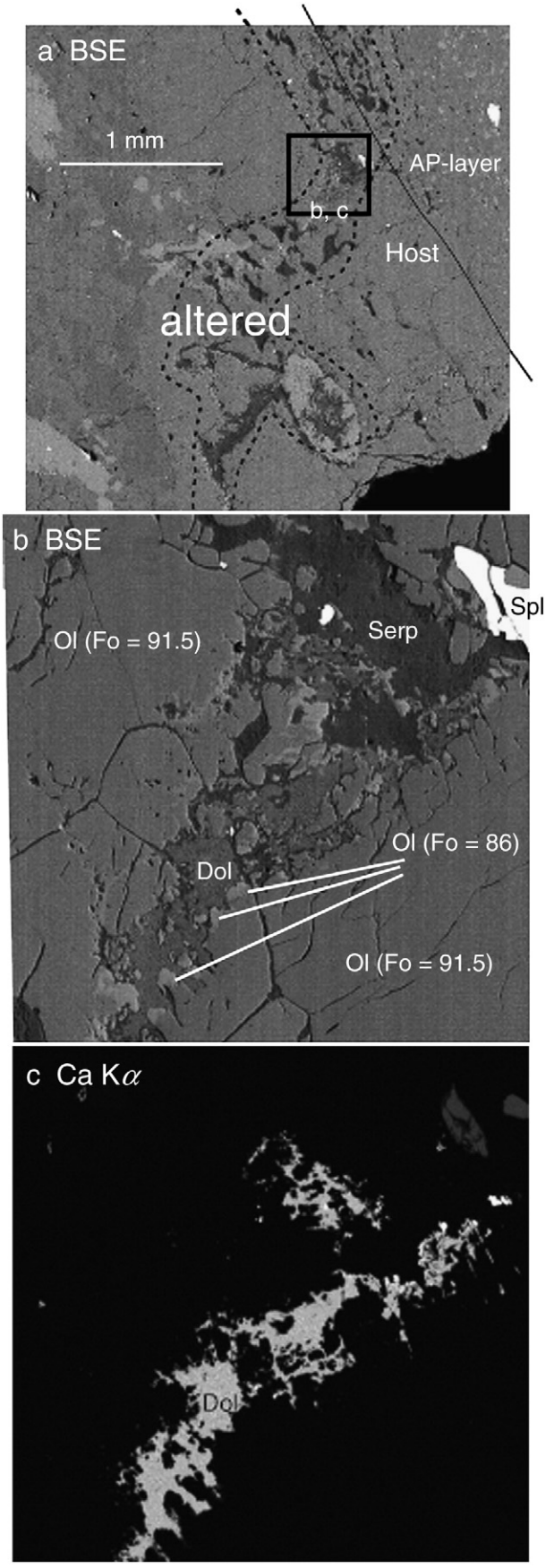

Fig. 3. Occurrence of large carbonate grains in an altered vein. (a) Back-scattered electron image of the altered vein containing large carbonate grains. (b) Back-scattered electron image showing occurrence of carbonate grains in a part of (a). Carbonate grains are partly in contact with Fe-rich olivine (brighter grains). (c) X-ray intensity maps in Ca of (b). Bright part means high content of Ca. AP-layer = apatite-rich layer, Fo = forsterite component, Dol = dolomite, Ol = olivine, Serp = serpentine, Spl = spinel.

Table 1
Whole-rock major- and trace-element compositions of the apatite-rich layer (A1) and the host rock (B1, C1, D1 and E1)

wt.%	A1	B1	C1	D1	E1
SiO_2	39.40	40.37	37.58	41.63	40.41
TiO_2	0.01	0.00	0.00	0.01	0.00
Al_2O_3	1.26	1.09	0.96	1.34	1.10
Fe_2O_3	7.41	7.98	8.09	7.79	8.05
MnO	0.11	0.12	0.11	0.11	0.11
MgO	42.58	44.44	44.80	43.53	45.18
CaO	1.70	1.11	1.48	1.36	1.27
Na_2O	0.19	0.14	0.16	0.20	0.16
K_2O	0.10	0.08	0.08	0.10	0.09
P_2O_5	0.43	0.01	0.01	0.01	0.01
Total	93.19	95.34	93.27	96.09	96.38
Mg/(Mg+Fe*)	0.891	0.888	0.887	0.888	0.888
Si/(Mg+Fe*) ppm	0.772	0.756	0.697	0.796	0.745
Sc	9.80	n.d.	10.01	10.16	11.72
Sr	235	n.d.	81.0	64.8	44.7
Y	2.78	0.88	0.63	0.57	0.40
Ba	30.8	n.d.	23.7	27.2	9.79
La	30.2	3.24	2.41	2.37	1.64
Ce	36.1	5.12	3.59	3.24	2.14
Pr	2.79	0.47	0.32	0.28	0.19
Nd	8.30	1.55	1.11	0.98	0.67
Sm	0.95	0.23	0.18	0.17	0.12
Eu	0.23	0.06	0.05	0.04	0.03
Gd	0.64	0.18	0.13	0.13	0.10
Tb	0.08	0.02	0.02	0.02	0.01
Dy	0.46	0.14	0.11	0.10	0.08
Ho	0.09	0.03	0.02	0.02	0.02
Er	0.26	0.10	0.07	0.07	0.05
Tm	0.04	0.02	0.01	0.01	0.01
Yb	0.25	0.11	0.08	0.08	0.06
Lu	0.04	0.02	0.01	0.01	0.01
Th	5.24	n.d.	0.36	0.46	0.35
U	1.24	n.d.	0.51	0.06	0.06

See Fig. 1 and text for details. Mg/(Mg+Fe*) and Si/(Mg+Fe*) are atomic ratios (Fe* is total iron).

(Table 1) were determined by an Inductively Coupled Plasma-Mass Spectrometer (ICP-MS) (Yokogawa HP 4500) at Nagoya University following the methods described by Takayanagi et al. (2000) and Takebe and Yamamoto (2003). About 50mg samples were digested with HF (1 ml)-$HClO_4$ (0.5 ml) mixture on a hot plate at 180 °C and were subsequently dissolved in 1.7M HCl. Chromian spinel did not completely dissolve in the solution, but this does not affect the concentrations of elements discussed in this paper because spinel is low in abundance (usually < 1 modal%) and does not incorporate much of these elements (e.g., Takazawa et al., 2003). The sample solution was subjected to cation chromatographic separation (Dowex 50WX8) of REEs from major elements and Ba. Finally, the sample solution was dissolved in 2% HNO_3 for ICP-MS analyses. Mixed standard solutions made from the individual REE oxides were used as external calibration standards for REE analyses. Standard solutions for trace elements other than REEs were made from a standard composite glass prepared by Yamamoto and Morishita (1997) for trace-element determinations by XRF. Interference of light REEs oxides on heavy REEs masses was corrected applying respective oxide factors of LREEs determined by the measurement of 20ppb LREE solutions. Both In and Bi were employed as internal standards. Analytical errors were estimated to be < 10% for Ba, Th and U, and < 3% for other elements including REEs. Precision and accuracy of GSJ JB-1 and USGS BCR-1 with the same analytical conditions appear in Yamamoto et al. (2005).

Major-element compositions of amphibole (Table 2) were determined by the Electron Microprobe analysis (EMPA: JEOL-JXA8800) at the Center for Cooperative Research of Kanazawa University following the procedure described in Morishita et al. (2003a,b). The analytical conditions were as follows: 20kV accelerating voltage, 20nA beam current and 3 μm beam diameter. Natural and synthetic minerals were used as calibration standards. The raw data were converted to wt.% with the JEOL software using ZAF corrections. Trace-element compositions (Li, Sc, Ti, V, Rb, Sr, Y, Zr, Nb, Cs, Ba, REE, Hf, Ta, Pb, Th, U) of amphiboles (Table 2) and apatites (Table 3) were determined using an ICP-MS (Agilent 7500S) equipped with an ArF excimer laser ablation system (193 nm, 5 Hz: MicroLas GeoLas Q-plus) at the Incubation Business Laboratory Center of Kanazawa University (Ishida et al., 2004). Ablation of an area with a diameter of 50 μm and 10 μm was required for amphibole and apatite, respectively. The peak of ^{42}Ca was monitored as internal standard, as described in Longerich et al. (1996), and the NIST SRM 612 and 610 glasses were used as the calibration standards for amphibole and apatite, respectively. These glasses were analyzed at the beginning of each batch of analyses (within 8 analyses) with a linear drift correction of standard intensities applied between each calibration. The element concentrations of glasses were taken from Pearce et al. (1997). Detailed analytical procedures, and the precision and accuracy of the data on NIST SRM 614 and BCR-2g reference standard glasses with the same analytical conditions appear in Morishita et al. (2005a,b).

For Sr- and Nd-isotope analyses (Table 4), three small pieces were selected. Two samples (T-X and T-1) containing AP-layer, similar to A1 of Fig. 1, and one peridotite (T-2) adjacent to the T-1, similar to B1 of Fig. 1. Note that the T-2 (host peridotite) contains fine-grained part where apatite and carbonate are found (Morishita et al., 2003b). Samples were subjected to sequential leaching using 0.15N HCl and 2.5N HCl, which dissolve carbonate and apatite, respectively (Griffin et al., 1988). This is confirmed by qualitative analyses of leachates using ICP-MS, which showed Ca, Mg, Sr with no P in 0.15N HCl and P in 2.5 HCl. One whole-rock sample containing AP-layer (T-1) and mineral separates (amphibole and apatite) by handpicking were also prepared for conventional chemical digestion procedures. It should be noted that it was impossible to eliminate the contamination of other minerals for the apatite fraction because of tiny grains. However other transparent minerals (mainly olivine and minor orthopyroxene) are very low in trace-element concentrations. Thus elemental contaminations from these minerals are neglected. For isotope analysis, Sr and Nd were separated using the cation resin and orthophosphaoric acid-coated Teflon beads. Isotopic measurements were made on a multi-collector thermal ionization mass spectrometer (Finnigan MAT 261) at the Ottawa-Carleton Geoscience Centre. The ratios for the Sr- and Nd-isotopes were normalized to $^{86}Sr/^{88}Sr$ of 0.1194 and $^{146}Nd/^{144}Nd$ of 0.7219. During the course of isotopic analysis, measurements of NBS987 and LaJolla gave $^{87}Sr/^{88}Sr$ of 0.710257 ± 22 (2σ, N = 8) and $^{143}Nd/^{144}Nd$ of 0.511880 ± 13 (2σ, N = 8).

Carbon and oxygen isotope compositions of dolomite were determined on the whole-rock powder mixed with 100% orthophosphoric acid. The sample was kept in vacuum at 25 °C for 24h to allow the removal of calcite, but no CO_2 was released during the period, confirming the absence of calcite in the sample. This is followed by the reaction of the mixture for 48h at 50 °C for the extraction of CO_2 from dolomite. The isotopic measurement of CO_2 was performed on a Delta XP and a Gas Bench II, both from Thermo Finnigan at the University of Ottawa.

In-situ isotope analyses of apatite were carried out on a polished section using a SHRIMP at the Hiroshima University. A ~ 5nA O_2^- primary beam at an energy of 10 keV was focused to a 10 μm-diameter area and the secondary ions were extracted with an acceleration voltage of 10 kV. The mass resolution was 5800 at 1% peak height of ^{208}Pb. Experimental details and the calibration of data using a reference apatite, "PRAP", from 1156Ma Prairie Lake complex in Canada are described in Sano et al. (1999a,b; 2000). Thirteen areas were analyzed from the apatite-rich part in one section. Uranium concentration, $^{238}U/^{206}Pb$, $^{207}Pb/^{206}Pb$, $^{206}Pb/^{204}Pb$ and $^{208}Pb/^{204}Pb$ ratios of apatite in the apatite-rich layer are listed in Table 5. Uncertainties of these concentrations are ± 30% based on the repeated measurements of the reference apatite. An isochron method is used, because of the generally lower ratio of radiogenic to common Pb in apatite.

Table 2
Major- and trace-element compositions of amphiboles

Host	Toward to Apatite-rich layer						Apatite-rich layer					
Anal. no. wt.%	#6	#8	#11	#13	#15	#17	#18	#24	#29	#34	#38	#39
SiO_2	45.62	45.45	45.61	45.51	45.57	45.42	45.54	45.75	45.04	45.28	44.56	45.29
TiO_2	0.41	0.35	0.39	0.37	0.37	0.40	0.36	0.35	0.36	0.42	0.35	0.33
Al_2O_3	11.07	11.66	11.21	11.18	11.46	11.15	11.27	11.21	10.81	11.06	11.13	10.90
Cr_2O_3	1.99	1.99	2.03	2.02	1.96	1.80	1.80	1.81	1.94	1.93	1.88	1.86
FeO	3.40	3.51	3.55	3.42	3.52	3.51	3.47	3.44	3.46	3.60	3.50	3.39
MnO	0.00	0.07	0.03	0.05	0.05	0.04	0.04	0.07	0.05	0.04	0.03	0.05
MgO	18.99	18.78	18.86	19.01	19.00	19.09	19.09	19.03	19.09	19.00	18.86	18.93
CaO	11.99	11.97	12.02	11.88	11.95	12.10	12.12	12.16	12.24	12.31	12.58	12.56
Na_2O	2.23	2.51	2.29	2.42	2.40	2.48	2.51	2.39	2.27	2.36	2.45	2.46
K_2O	0.90	0.87	0.90	0.88	0.75	0.69	0.72	0.76	0.74	0.74	0.72	0.69
total	96.62	97.17	96.89	96.73	97.00	96.67	96.91	96.96	96.02	96.73	96.05	96.46
Mg#	0.909	0.905	0.904	0.908	0.906	0.906	0.907	0.908	0.908	0.904	0.906	0.909
K# ppm	0.210	0.186	0.206	0.194	0.170	0.155	0.159	0.173	0.177	0.172	0.162	0.157
Li	0.54	0.83	0.53	<0.6	0.71	<0.6	<0.5	<0.6	<0.6	<0.5	<0.6	<0.5
Sc	75	83	73	74	75	80	80	79	77	82	84	79
Ti	2584	2714	2496	2490	2607	2571	2610	2617	2584	2672	2730	2624
V	338	357	328	328	329	345	350	347	349	368	364	352
Rb	17	15	18	15	11	3.8	4.3	6.0	5.7	6.2	5.3	5.8
Sr	602	686	691	748	839	875	907	933	888	977	930	890
Y	6.0	7.9	7.8	9.8	12	22	21	22	22	25	24	23
Zr	29	32	29	29	29	30	30	31	30	32	32	30
Nb	2.2	2.9	2.5	3.7	4.2	7.3	7.4	8.5	8.5	11	8.7	8.5
Cs	0.04	0.02	0.03	0.02	0.02	<0.02	<0.02	<0.02	<0.02	<0.02	<0.02	<0.02
Ba	183	247	238	290	190	198	227	239	228	276	237	231
La	28	33	33	38	47	57	55	57	57	57	61	56
Ce	44	53	52	62	88	121	116	121	122	126	128	122
Pr	3.6	4.6	4.3	5.5	7.8	12	12	12	12	13	13	12
Nd	11	15	13	18	25	42	39	41	42	47	45	43
Sm	1.7	2.2	2.1	2.6	3.3	6.1	5.9	6.2	6.2	7.2	6.6	6.3
Eu	0.49	0.59	0.57	0.72	0.92	1.7	1.6	1.7	1.8	1.9	1.8	1.7
Gd	1.2	1.5	1.4	1.8	2.5	4.4	4.3	4.5	4.5	5.5	5.0	4.9
Dy	0.93	1.2	1.1	1.5	2.0	3.5	3.3	3.5	3.6	4.3	4.0	3.7
Er	0.59	0.76	0.76	0.86	1.1	2.1	2.0	2.0	2.0	2.3	2.2	2.1
Yb	0.74	0.95	0.86	0.97	1.4	2.0	2.0	2.1	2.2	2.2	2.2	2.2
Lu	0.11	0.14	0.13	0.18	0.20	0.28	0.29	0.32	0.31	0.32	0.32	0.30
Hf	0.68	0.81	0.75	0.66	0.71	0.81	0.82	0.77	0.74	0.85	0.87	0.81
Ta	0.09	0.12	0.11	0.11	0.13	0.14	0.16	0.16	0.16	0.18	0.17	0.17
Pb	3.0	3.0	2.9	3.0	3.2	3.0	3.3	3.4	3.2	3.5	3.3	3.3
Th	2.3	2.1	2.4	2.2	2.1	2.4	2.6	2.7	2.6	2.9	3.0	2.5
U	0.32	0.29	0.30	0.31	0.27	0.25	0.32	0.41	0.35	0.42	0.39	0.32

FeO* is total iron. Mg# = Mg/(Mg + Fe^{2+}) atomic ratio, K# = K/(K + Na) atomic ratio. Anal. No. = name of analyzed point. Detection limit was calculated for each analysis.

4.2. Whole-rock chemical compositions

The slice containing AP-layer (A1) is higher in CaO and P_2O_5 contents than the surrounding peridotitic ones (Table 1). Whole-rock major-element compositions of peridotite samples are controlled by modal mineralogy, because of the large grain size of minerals, in particularly, orthopyroxene (~ 2 mm) and amphibole (~ 2 mm). For example, the D1 slice contains high Al_2O_3 and CaO contents because of the abundant amphibole in the slice.

All samples show high LREE relative to HREE and a positive Sr anomaly in chondrite-normalized patterns (Fig. 4). The A1 slice contains high concentrations of REE, U, Th and Sr than the other slices. The A1 slice shows higher LREE/HREE ratio ((La/Yb) n = 82) than the other ones ((La/Yb) n = 18–19). The whole-rock REE concentrations increase toward the AP-layer, but chondrite- and primitive mantle-normalized REE and trace-element patterns are similarly fractionated among the different samples.

4.3. Mineral compositions

Amphibole is pargasite following the classification of Leake et al. (1997). All amphibole grains contain high LREE relative to HREE (Fig. 5) and show a positive Sr anomaly with low concentrations of HFSE (Fig. 6). The total REE concentrations in amphiboles increase closer to the AP-layer whereas the HFSE concentrations do not show any change (Fig. 5). Amphiboles in the AP-layer show lower K/(K + Na) ratios than those in the host peridotite. Zanetti et al. (1999) found Nb-enriched edenite in their apatite-bearing samples (Fig. 6), but we did not find high Nb contents (< 11ppm) in amphibole during our study.

Apatite grains show extremely high LREE relative to HREE with low concentrations of HFSE relative to REE (Fig. 7). The HREE concentrations are positively correlated with Th (50–250ppm) and U (25–75ppm). Trace-element characteristics of apatite in the AP-layer are similar to those associated with the metasomatized wall-rock peridotites, “Apatite A”, of O'Reilly and Griffin (2000).

4.4. Isotopic compositions

Strontium and Nd-isotope compositions are calculated at 215Ma (Fig. 8), the apatite age obtained in this study (see below). The initial isotope compositions for the samples, particularly carbonates and apatite, are assumed to be similar to the present values because of high Sr/Rb and Nd/Sm (e.g., Tsuboi, 2005). Carbonates in an AP-layer sample (T-X) that contains carbonate aggregate show high $^{87}Sr/^{86}Sr$ (0.70893) and low $^{143}Nd/^{144}Nd$ (0.51235) compared to whole-rock (0.70505 and 0.51264) and metasomatic minerals from AP-layer T-1 and its host peridotite T-2 (0.705 and 0.5125–0.5126) (Table 4).

Carbon isotope composition and $\delta^{18}O$ values of the carbonate in the sample T-X are − 3.5‰ and + 16.7‰, respectively (Fig. 9).

Table 3
Trace-element compositions of apatites

No. ppm	This study							Durango		NIST612	
	1–1	2–7	3–29	4–10	5–14	6–15	6–19	(*N*=5)	STD	(*N*=4)	STD
Li	<8	<6	<6	<9	<5	<6	<6	<6		43	
Si	<2000	<3000	<3000	<2000	<3000	<3000	<3000	<3000		340000	9600
Sc	<0.6	<0.8	<0.9	<0.7	<0.9	<0.9	<0.9	<1		38	3
Ti	<4	<7	1.68	<6	<7	<7	<8	<11		40	12
V	3.1	8.7	3.4	10	6.9	6.1	3.4	35	2	37	3
Rb	<0.3	<0.4	<0.4	<0.3	<0.4	<0.4	<0.4	<0.6		32	2
Sr	9700	9300	10500	10500	9600	8800	9300	485	14	77	6
Y	34	57	35	40	42	61	41	521	28	37	2
Zr	<0.1	0.93	<0.1	0.18	<0.1	0.97	0.26	0.48	0.09	37	3
Nb	<0.04	<0.1	<0.1	<0.1	<0.1	<0.1	<0.1	<0.1		35	2
Cs	<0.2	<0.2	<0.2	<0.2	<0.2	<0.2	<0.02	<0.2		42	4
Ba	0.86	1.20	0.62	1.08	0.81	0.85	1.21	<0.5		39	5
La	1400	2300	2100	2000	1800	1600	1700	3530	120	38	3
Ce	1600	2400	2100	2100	2000	2000	1900	4200	130	39	3
Pr	103	158	135	134	125	140	118	343	11	37	3
Nd	262	398	325	325	322	369	301	1080	30	36	3
Sm	22	34	26	28	28	33	27	144	8	36	3
Eu	4.6	7.3	5.7	6.2	6.4	7.9	5.5	16	1	37	2
Gd	12	20	13	15	15	19	13	119	7	36	3
Dy	5.0	10	6.0	7.0	7.4	11	7.1	86	5	34	2
Er	2.4	4.9	3.2	3.6	3.4	5.4	3.5	44	1	36	3
Yb	2.4	4.6	1.8	2.5	3.0	4.2	2.9	34	1	39	3
Lu	0.30	0.77	0.46	0.27	0.29	0.51	0.42	4.0	0.3	37	2
Hf	<0.3	<0.3	<0.2	<0.3	<0.3	<0.2	<0.2	<0.5		36	4
Ta	<0.1	<0.1	<0.1	<0.1	<0.1	<0.1	<0.1	<0.1		32	2
Pb	12	14	16	11	12	11	9	1.1	0.4	38	4
Th	62	257	57	58	57	200	57	228	17	37	3
U	32	76	23	25	25	75	37	11.4	0.5	38	3

Detection limit was calculated for each analysis. The values of NIST 612 and the Durango apatite, widely used as a standard for fission-track and (U–Th)/He dating (e.g., McDowell et al., 2005), are also shown.

4.5. Apatite U–Pb–Th data

A three-dimensional linear regression of the data on the $^{238}U/^{206}Pb$–$^{207}Pb/^{206}Pb$ projection (Fig. 10a; Wendt, 1989) intersects the Tera-Wasserburg Concordia, yielding an age of 215 ± 35Ma (MSWD = 2.4). Fig. 10b shows a correlation between $^{232}Th/^{204}Pb$ and $^{208}Pb/^{204}Pb$ ratios of apatite. A least-squares fit (York, 1969) gives the ^{232}Th–^{208}Pb* (decay product) isochron age of 254 ± 78 Ma (MSWD = 2.3). This age is consistent with the Tera-Wasserburg concordia-constrained linear three-dimensional isochron age. Uranium concentrations determined with a SHRIMP show a significant range from 30ppm to 200ppm, in agreement with LA-ICP-MS data, and show a negative correlation with $^{204}Pb/^{206}Pb$ and $^{204}Pb/^{207}Pb$ rations (Table 5), suggesting a variable contribution of common Pb to the sample and/or a supply of variable U/Pb. Irrespective of the contribution of common Pb, the age of apatite obtained using a SHRIMP (215 ± 35Ma and 254 ± 78Ma) is comparable to the K–Ar age (240 ± 41Ma) obtained for the sample studied by Matsumoto et al. (2005).

5. Discussion

5.1. Late carbonate formation/recrystallization

Initial $^{87}Sr/^{86}Sr$ value for carbonate (0.7089) in the carbonate aggregate-bearing sample (T-X) is distinctly higher than the metasomatic minerals and whole-rock (these are around 0.705) in T-1 (AP-layer) and T-2 (the host rock adjacent T-1) (Fig. 8). In particular, $^{87}Sr/^{86}Sr$ value for carbonate form T-2 (the host) is similar to the other data. The carbonate aggregate-bearing sample (T-X) yielded the carbon isotope composition of − 3.5‰, which is higher than the so-called mantle value of − 6‰ and typical carbonatite values (which span from of − 4 to − 8‰; Keller and Hoefs, 1995) (Fig. 9), and lower than the marine carbonate value of ~ 0‰. The carbon isotope composition of graphite intergrowth within phlogopite from the Finero is higher (16.1 to − 10.4‰) than the studied values (Ferraris et al., 2004). The $\delta^{18}O$ value of + 16.7 for the T-X sample is high compared to the mantle carbonates and carbonatite of + 5 to + 10‰ (Keller and Hoefs, 1995). The carbonate in the T-X may be formed or equilibrated with aqueous fluids at low temperatures because carbonates would easily exchange oxygen isotopes with aqueous fluids at low temperatures (Keller and Hoefs, 1995) (Fig. 9). This interpretation is supported with its close association with serpentine and talc. We, therefore, conclude that the carbonate aggregate crystallized later at low temperatures, whereas dolomite coexisting with olivine was formed at the same time of formation of the apatite.

5.2. Relationships between the AP-layer and "nominally" apatite-free peridotites in the Finero massif

Major-element compositions of the Finero peridotites indicate an origin for most peridotites as residue after partial melting

Table 4
Sr- and Nd-isotope compositions of the samples

Sample no.	Phase	$^{87}Sr/^{86}Sr$ (present)	$^{87}Rb/^{86}Sr$	$^{87}Sr/^{86}Sr$ (215 Ma)	$^{143}Nd/^{144}Nd$ (present)	$^{147}Sm/^{144}Nd$	$^{143}Nd/^{144}Nd$ (215 Ma)
AP-layer							
T-X	Leachate (carbonate)	0.708930			0.512346		
T-1	Whole rock	0.705051			0.512623		
	Amphibole*	0.704704	0.0327	0.704604	0.512642	0.1004	0.5125
	Apatite*	0.704952	<0.001	0.70468*	0.51257	0.04858	0.512501
Host peridotite							
T-2	Leachate (carbonate)	0.705022		0.705022			
T2–2.5N	Leachate (apatite)	0.705289		0.705289			

Table 5
U concentrations, $^{238}U/^{206}Pb$, $^{207}Pb/^{206}Pb$, $^{204}Pb/^{206}Pb$, $^{204}Pb/^{208}Pb$ and $^{232}Th/^{208}Pb$ ratios of apatites within the apatite-rich layer

Sample no.	U (ppm)	$^{238}U/^{206}Pb$		$^{207}Pb/^{206}Pb$		$^{204}Pb/^{206}Pb$		$^{204}Pb/^{208}Pb$		$^{232}Th/^{208}Pb$	
Finero01.01	34	2.51	(0.32)	0.656	(0.047)	0.0442	(0.0058)	0.0216	(0.0036)	30.6	(10)
Finero01.02	53	5.02	(0.69)	0.665	(0.032)	0.0392	(0.0039)	0.0216	(0.0024)	10.7	(2.2)
Finero01.03	74	5.80	(0.47)	0.689	(0.015)	0.0428	(0.0033)	0.0242	(0.0020)	12.4	(1.7)
Finero17.01	189	10.59	(0.52)	0.555	(0.018)	0.0278	(0.0016)	0.0154	(0.0010)	39.9	(3.1)
Finero19.1	202	11.80	(0.43)	0.509	(0.010)	0.0196	(0.0027)	0.0112	(0.0016)	42.5	(2.6)
Finero19.2	86	9.21	(0.93)	0.549	(0.010)	0.0317	(0.0021)	0.0203	(0.0014)	6.8	(1.1)
Finero19.3	132	8.00	(0.71)	0.558	(0.015)	0.0354	(0.0025)	0.0221	(0.0017)	23.7	(3.1)
Finero23.1.1	180	14.7	(1.2)	0.499	(0.010)	0.0270	(0.0023)	0.0171	(0.0015)	46.0	(6.5)
Finero23.1.2	183	12.0	(1.3)	0.523	(0.020)	0.0284	(0.0027)	0.0185	(0.0019)	31.1	(5.3)
Finero23.1.3	160	10.67	(0.81)	0.568	(0.017)	0.0273	(0.0021)	0.0173	(0.0014)	25.7	(2.8)
Finero23.2.1	31	2.34	(0.24)	0.731	(0.017)	0.0491	(0.0020)	0.0265	(0.0012)	4.83	(0.75)
Finero23.2.2	167	9.36	(0.49)	0.563	(0.017)	0.0334	(0.0018)	0.0199	(0.0012)	25.0	(2.2)
Finero23.2.3	155	8.60	(0.87)	0.647	(0.029)	0.0295	(0.0020)	0.0145	(0.0011)	28.3	(4.4)

Numbers next to each isotope ratio is error (one sigma) estimated by counting statistics and calibration.

(Hartmann and Wedepohl, 1993). Then the Finero peridotite subsequently suffered intense metasomatic modifications by the infiltration of a melt or fluid enriched in highly incompatible elements, resulting in the formation of amphibole and phlogopite (Exley et al., 1982; Voshage et al., 1987; Hartmann and Wedepohl, 1993; Zanetti et al., 1999; Prouteau et al., 2001). Whether the AP-layer was formed in a single metasomatic event for most metasomatized, phlogopite–amphibole-rich peridotites remains to be established.

Radiogenic isotopes are useful tools to constrain the sources of metasomatic agents. The Finero phlogopite-rich peridotites are characterized by high contents of Sr, Rb and Ba (Hunziker and Zingg, 1982), and high $^{87}Sr/^{86}Sr$ ratios (Voshage et al., 1987; Hartmann and Wedepohl, 1993) (Fig. 8). Voshage et al. (1987) show a negative

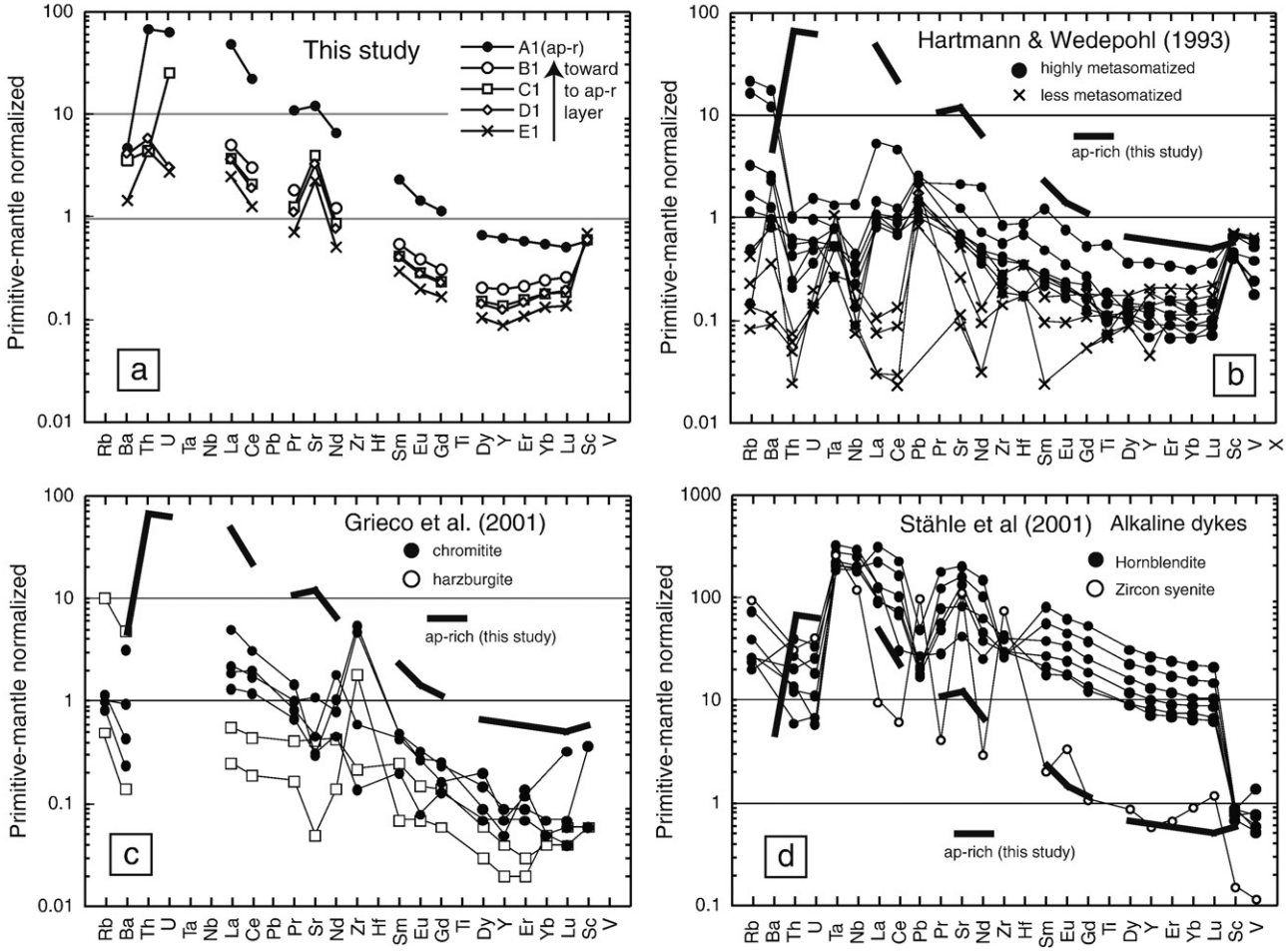

Fig. 4. Primitive mantle-normalized trace-element variation diagrams for whole-rock compositions of the Finero massifs. The value of the primitive mantle is from McDonough & Sun (1995). (a) This study. See Fig. 1 for the sample positions (A1 containing the apatite-rich layer and the host B1, C1, D1 and E1) analyzed for whole-rock compositions in the sample. (2) "Nominally" apatite- and carbonate-free peridotites of Hartmann and Wedepohl (1993). (3) Zircon-bearing chromitite and related peridotites of Grieco et al. (2001). (4) Alkaline dykes intruded in the Finero massif (Stähle et al., 2001). ap-r and ap-rich = apatite-rich layer.

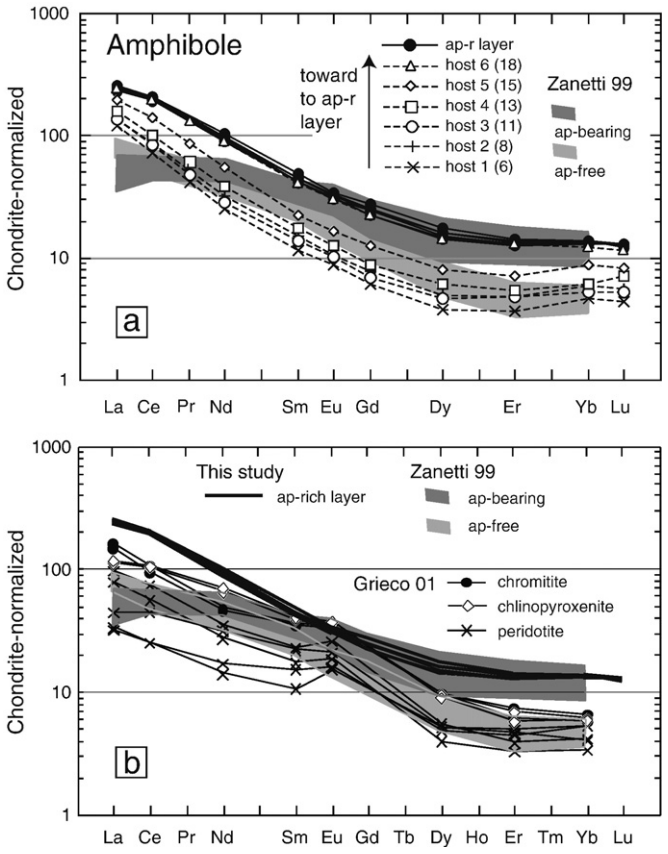

Fig. 5. Chondrite-normalized REE patterns for amphiboles in the Finero massif. The chondrite value is from McDonough and Sun (1995). (a) This study and compositional range from "apatite- and carbonate-bearing lithologies" of Zanetti et al. (1999). (b) Zircon-bearing chromitite and related rocks of Grieco et al. (2001). Data of apatite-rich layer and compositional ranges of "apatite- and carbonatite-bearing lithologies of Zanetti et al. (1999) are also shown. ap-r = apatite-rich layer.

correlation between $^{143}Nd/^{144}Nd$ and $^{87}Sr/^{86}Sr$ and proposed mixing between phlogopite-free peridotites and paragneiss in the Ivrea Zone. Previous isotopic data from phlogopite-rich peridotites suggest a contribution of an isotopically evolved metasomatic agent, probably derived from the slab-derived components (Voshage et al., 1987; Cumming et al., 1987; Hartmann and Wedepohl, 1993). Hartmann and Wedepohl (1993) suggested that amphibole separates in the Finero peridotites show two types of Sr-isotopic signatures. One type has relatively low ($^{87}Sr/^{86}Sr$) i, around 0.7030 (at 215Ma), whereas the second one contains radiogenic Sr isotope signature, 0.706–0.708 (at 215Ma) (Fig. 8). Although rocks in both types contain phlogopite, high ^{87}Sr samples contain high K_2O content and LREE/HREE ratios in the whole rocks compared to low ^{87}Sr samples. The Sr and Nd-isotope compositions in both AP-layer and its host rock (T-1 and T-2) have a bulk Earth-like signature (Zindler and Hart, 1986), and are, therefore, different from the values for "nominally" apatite-free phlogopite-rich peridotites (Voshage et al., 1987; Hartmann and Wedepohl, 1993). It is concluded that the metasomatic agent for apatite and carbonate formation was different from that for phlogopite formation. A distinct agent for apatite-carbonate formation is further supported by the recent geochemical data reported by Matsumoto et al. (2005) and Raffone et al. (2006). Matsumoto et al. (2005) reported distinct noble gas isotope compositions from a sample containing AP-layer (similar to sample T-1 in Fig. 1). Raffone et al. (2006) recently investigated the concentrations of Li and B in clinopyroxene grains of "apatite-bearing domains" of Zanetti et al. (1999), and suggested that clinopyroxene data plot in the field of non-metasomatized Sub-Continental Depleted Mantle of Ottolini et al. (2004), whereas the data from phlogopite–peridotites plot in the field for arc or crust.

5.3. Relationships between the Ap-layer and other apatite-bearing lithologies in the Finero massif

As suggested above, there have been several studies on apatite- and carbonate-bearing samples from the Finero phlogopite–peridotites, such as the "apatite- and carbonate-bearing regions" (wehrlitic in modal composition: Zanetti et al., 1999; Raffone et al., 2006), the "apatites and/or carbonates-bearing chromitites (Ferrario & Garuti,

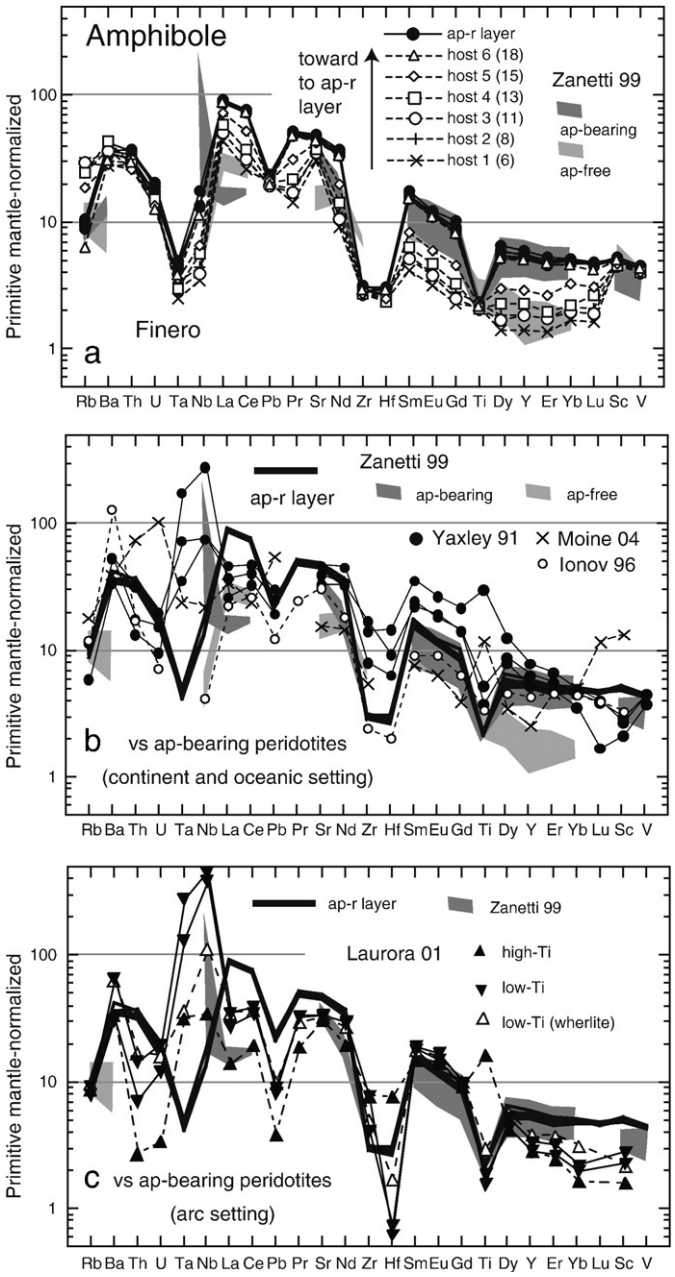

Fig. 6. Primitive mantle-normalized trace-element variation diagrams for amphiboles in this study (a), and other apatite and/or carbonate-bearing xenoliths in continent and oceanic settings (b) and arc setting (c). Compositional range of amphibole from the apatite- and carbonate-bearing lithologies of Zanetti et al. (1999) are also shown. Data of continent and oceanic settings are from Yaxley et al. (1991) (Yaxley 91), Ionov et al. (1996) (Ionov 96) and Moine et al. (2004) (Moine 04). Data of arc setting from Laurora et al. (2001) (Laurora 01).

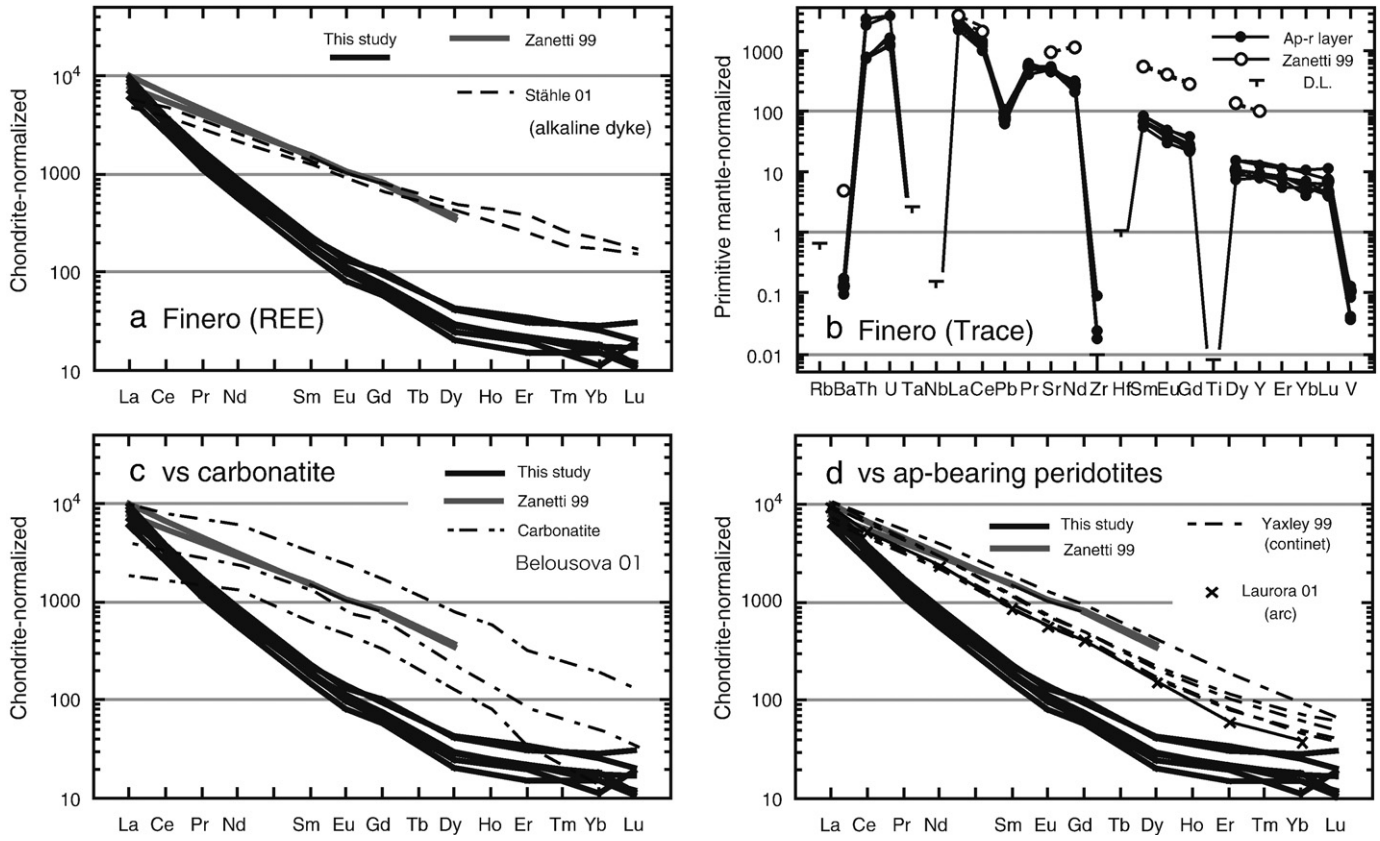

Fig. 7. Chondrite-normalized REE patterns and primitive mantle-normalized trace-element variation diagrams of apatite in the Finero (a, b), carbonatite (c) and other apatite-bearing peridotites (d). Zanetti 99 = Zanetti et al. (1999), Stähle 01 = Stähle et al. (2001), Belousova 02 = Belousova et al. (2002), Yaxley 99 = Yaxley and Kamenetsky (1999), Laurora 01 = Laurora et al. (2001).

1990; Zaccarini et al., 2004), and the studied sample (Morishita et al., 2003a,b; Matsumoto et al., 2005). The chromitite contains Zr–Th–U-rich minerals including zircon (Zaccarini et al., 2004). In addition to these peridotitic samples, alkaline dykes in the massif contain apatite and/or carbonate (Stähle et al., 1990, 2001).

Zanetti et al. (1999) and Morishita et al. (2003b) suggested that apatite- and carbonate-bearing rocks were metasomatized by carbonatitic agents that formed through immiscible separation from SiO_2-rich fluids/melts possibly during active subduction. Zaccarini et al. (2004) proposed that apatites and/or carbonates associated with zircon, zirconolite and Zr–Th–U minerals in some chromitites were formed from metasomatic agents related to carbonatites during the upwelling of a mantle plume in a continental rift. However, the genetic relationships between apatite- and carbonate-bearing rocks in the Finero massif have never been, however, discussed before.

Whole-rock trace-element compositions of the AP-layers and the host peridotites are characterized by high LILE contents and low HFSE concentrations. Extremely high concentration of REE and high LREE/HREE ratio with depletion of HFSE of the whole-rock compositions (Fig. 4) and minerals (Figs. 5, 6 and 7) in the AP-layer are different from those of other lithologies in the Finero phlogopite–peridotites. The whole-rock trace-element compositions are, however, strongly controlled by the local concentration of apatite in the case of the studied samples. Mineral compositions are suitable for further discussions on the relationships between apatite-bearing lithologies in the Finero massif.

Minerals in the apatite-bearing lithologies are generally characterized by high REE contents with high LREE/HREE ratio, which are the same as those in other apatite-bearing lithologies. The LREE/HREE ratio of minerals is, however, much higher in the AP-layer than other apatite-bearing lithologies (Figs. 5 and 7). Furthermore, Nb–Ta-rich amphibole (Zanetti et al., 1999) and HFSE-rich minerals (Grieco et al., 2001; Zaccarini et al., 2004) have never been found in the AP-layer. These differences between samples may be explained by either an introduction of a distinct metasomatic agent to each lithology, or a

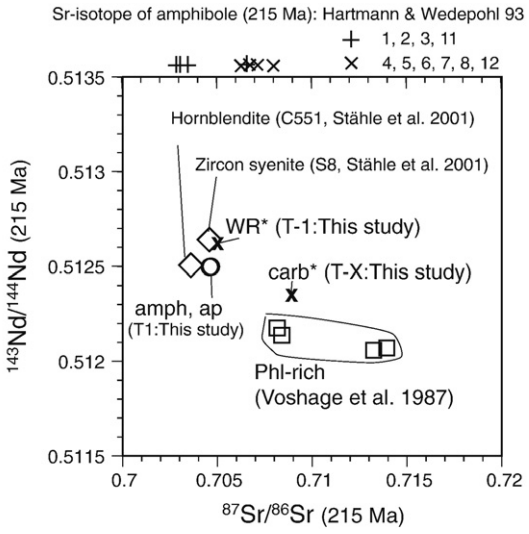

Fig. 8. $^{143}Nd/^{144}Nd$ vs $^{87}Sr/^{86}Sr$ at 215 Ma. The data for phlogopite-rich peridotites and alkaline dykes intruded in the Finero massif are from Voshage et al. (1987) and Stähle et al. (2001), respectively. Strontium isotopic data of amphibole in "nominally" apatite- and carbonate-free peridotites (Hartmann and Wedepohl, 1993) are also shown in the upper part of the diagram. The data indicated by X have no age corrections. ap = apatite, amph = amphibole, carb = carbonate, WR = whole-rock, Phl = phlogopite.

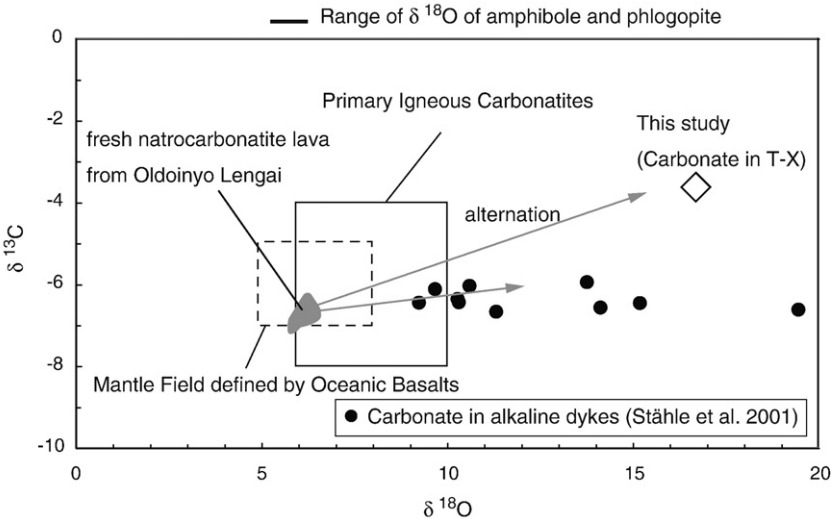

Fig. 9. Carbon and oxygen isotopic compositions of the carbonate-aggregate bearing sample (T-X), and carbonate in alkaline dykes intruded in the Finero massif (Stähle et al., 2001). See the text for more detailed explanations. Compositional range of fresh natrocarbonatite lava from Oldoinyo Lengai and arrows leading to data of altered natrocarbonatites are also shown (Keller and Hoefs, 1995).

distinct stage of the same metasomatic event. The apatite age (215 ± 35Ma) obtained in this study is comparable to the zircon ages for chromitites (204 and 207Ma of Von Quadt et al., 1993; 208 Ma of Grieco et al., 2001) and to the age for alkaline dykes (220–225Ma) (Stähle et al., 1990, 2001). Similar ages reported from the related rocks indicate that the apatite–carbonate-bearing lithologies were formed during a single metasomatic event, probably related to the Triassic magmatic activity reported in and around the Finero mafic–ultramafic complex.

Many studies of metasomatized peridotites have revealed that metasomatic agents drastically change their compositions during interactions with the rocks, as a result of chromatographic effects (Navon and Stolper, 1987; Zanetti et al., 1996) and precipitation of accessory minerals (e.g., Bodinier et al., 1990; Vannucci et al., 1995; Bedini et al., 1997; Laurora et al., 2001; Ionov et al., 2002; Bodinier et al., 2004; Rivalenti et al., 2004; Ionov et al., 2006; Kaeser et al., 2007). Relatively high LREE/HREE ratio in metasomatic minerals in the AP-layer can be explained by chromatographic fractionation. During reaction with the host rock, a metasomatic agent will become progressively enriched in incompatible elements as a function of distance from the source (e.g., Navon and Stolper, 1987; Zanetti et al., 1996). In addition to this, HFSEs-rich minerals and Th–U minerals are found in chromitites containing apatite in the Finero (Zaccarini et al., 2004). These minerals produce a significant elemental fractionation in the residual metasomatic agent (Bodinier et al., 1996). For example, if zircon, which would preferentially incorporate HFSE and HREE (Rubatto, 2002 and references therein), is formed during the reaction between host peridotites and a metasomatic agent, the fractionated metasomatic agent will be depleted in HFSEs and have high LREE /HREE ratio. These geochemical signatures, high-HREE/HREE ratio with depletion of HFSEs, are qualitatively consistent with those expected for the metasomatic agent for the formation of the AP-layer. Variable contents of HFSE in amphibole can be also explained by the evolution of metasomatic agents during the precipitation of metasomatic minerals and reaction with the host rock as discussed above. It is now well known that amphibole is relatively high in $D_{Nb}^{amph/melt}$ values, particularly in Ti-depleted systems (Tiepolo et al., 2001). An evolved metasomatic agent will thus progressively be deplete in HFSEs during the formation of metasomatic amphibole, resulting in the formation of Nb-depleted amphiboles further far from the source (Zanetti et al., 1996; Ionov et al., 2002; Kaeser et al., 2007). Elimination of Sr positive anomaly in amphiboles of the AP-layer is also likely consistent with the calculated model of Ionov et al. (2002), which

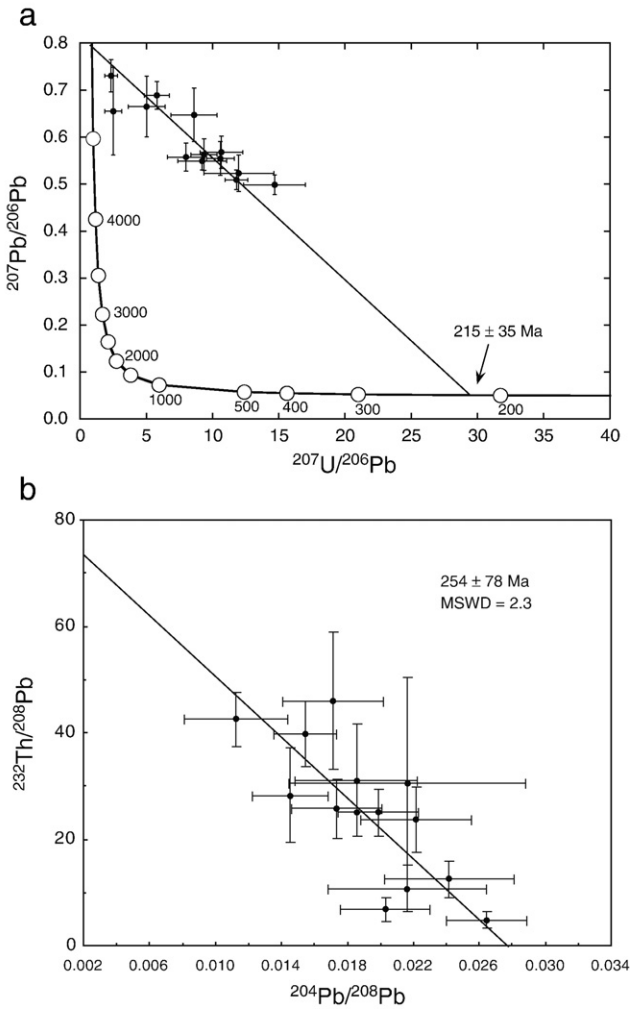

Fig. 10. U–Th–Pb isotope systematics in apatites. (a) Three-dimensional linear regressions of apatite for the total Pb/U isochron. All data are projected on the $^{238}U/^{206}Pb$–$^{207}Pb/^{206}Pb$ plane. The linear regressions were conducted as constrained to intersect the Tera-Wasserburg concordia by using Isoplot/Ex (Ludwig, 1998). (b) Correlation of $^{232}Th/^{208}Pb$ and $^{204}Pb/^{208}Pb$ ratios of apatite in the apatite-rich layer. A dotted line shows the best fit by the York method.

predicted the elimination of Sr positive anomaly in the sample far from the metasomatic agent.

In conclusion, we suggest that the metasomatic processes starting from one initial metasomatic agent might locally generate a compositionally distinct apatite-bearing lithology at a different stage during a single metasomatic event. The studied AP-rich layer therefore was a later product from such an evolved metasomatic agent after the formation of other apatite–carbonate-bearing lithologies with HFSE-rich minerals.

5.4. Implications for metasomatic agent for the formation of apatite-bearing lithologies in the Finero massif

Strong enrichments of LILEs and significant depletions in HFSEs of the whole-rock samples have been considered as a possible evidence for chemical interaction between peridotite and carbonatitic melts (Dautria et al., 1992; Hauri et al., 1993; Rudnick et al., 1993). The AP-layer has similar trace-element characteristics as that of the carbonatite and/or peridotites metasomatized by carbonatitic melts (Figs. 4, 6 and 7). However, there are notable differences in both petrology and geochemistry between carbonatite metasomatized peridotites and the studied AP-layer. Peridotites metasomatized by carbonatites contain high CaO/Al_2O_3 (> 2) and Na_2O/Al_2O_3 (> 0.2) ratios due to the formation of secondary clinopyroxene at the expense of orthopyroxene (e.g., Yaxley et al., 1991; Dautria et al., 1992; Hauri et al., 1993; Rudnick et al., 1993; Yaxley et al., 1998). The AP-layer, however, show low CaO/ Al_2O_3 (1.3), and Na_2O/Al_2O_3 (0.15). The close association of secondary orthopyroxene and amphiboles with apatite and carbonate in the AP-layer (Fig. 2) \suggest that the metasomatic agent was saturated with orthopyroxene component and was high in H_2O. Moreover, Cl content of apatite in carbonatite (e.g., Seifert et al., 2000; Bühn et al., 2001; Ahijado et al., 2005; Brassinnes et al., 2005) as well as carbonatite metasomatized peridotite (Hauri et al., 1993; Rudnick et al., 1994; Chalot-Prat and Arnold, 1999; Rosatelli et al., 2007) is usually very low. High Cl concentration of apatite in the studied sample seems to be of slab origin, because subducted slabs, in generally, will be rich in chloride during the hydrothermal alteration of the seafloor before subduction (Philippot and Selverstone, 1991; Scambelluri et al., 1997; Philippot et al., 1998). We, however, emphasize that the high-Cl apatite in the metasomatized peridotites cannot provide definite evidence of slab-derived origin because the chemical signatures of the metasomatic agent for the formation of the AP-layer had been extensively modified from those of the parent metasomatic agents due to interaction with the host peridotites. Fluorine and chlorine contents of apatite in metasomatized peridotites vary probably due to the reflecting metasomatic stages even in a single metasomatic event (Kaeser et al., 2007).

It is difficult to constrain the geochemical features of the "parent" metasomatic agent for the apatite-bearing lithologies because the metasomatic agents responsible for the formation of the apatite-bearing lithologies in Finero probably evolved with time, as discussed above. We suggest that the lithologies with relatively HFSE-rich minerals were formed by the interaction with an earlier metasomatic agent than with the AP-layer. It should be noted that the trace-element characteristics of apatite in the "alkaline dykes" (Fig. 4d), are similar to those in the apatite- and carbonate-bearing regions of Zanetti et al. (1999). Furthermore, the Sr–Nd-isotopic compositions of these "alkaline dykes" are similar to those of the studied samples (Fig. 8). However, the alkaline dykes (hornblendites) have unique geochemical characteristics with a wide range of chemical compositions, e.g., 27–45 wt.% SiO_2, 1–11 wt.% CO_2, probably in accord with a cumulus origin rather than melt compositions. Despite these difficulties, Sr-isotopic compositions of the AP-layer and the alkaline dikes indicate that slab-derived components were less abundant in the metasomatic agent that formed these rocks compared to that of the apatite-free phlogopite–peridotite, as already suggested by Stähle et al. (1990, 2001) and Raffone et al. (2006). Further studies on careful comparisons of the studied rocks with these "alkaline dykes" are warranted to constraint the origin and the tectonic setting responsible for the formation of the metasomatic agent of the apatite-bearing lithologies in the Finero massif.

6. Conclusions

We determined the geochemical characteristics (major, trace and isotopic compositions) of apatite-rich peridotite layer (AP-layer) and compared them with the "nominally" apatite-free lithologies and other apatite-bearing lithologies in the Finero peridotite massif. The results are summarized below.

(1) Strontium and Nd-isotopic compositions of minerals in an AP-layer and its host peridotites show bulk silicate Earth-like signature which is different from the ancient crustal signature for phlogopite-rich peridotites.
(2) Sr, Nd, C, and O isotope compositions for carbonate indicate that carbonate aggregates in serpentine-talc veinlets were likely formed late at low-temperatures after the formation of the AP-layers.
(3) The AP-layer is characterized by high LILE contents with high LREE/HREE ratios, and low HFSE concentrations. Furthermore, they show low CaO/Al_2O and Na_2O/Al_2O_3 ratios, which are different from the peridotites metasomatized by carbonatite melt. The metasomatic agents for the formation of the AP-layer was highly evolved orthopyroxene-saturated hydrous fluids/melts after the formation of other apatite- bearing rocks previously reported in the Finero massif where HFSE-rich minerals were formed due to the interaction with surrounding peridotites.
(4) The *in-situ* apatite SHRIMP ages (215±35 Ma) of the studied sample imply that the metasomatism is synchronous with the Triassic magmatic activity around the Finero massif.

Acknowledgements

We acknowledge the support from Kanazawa University 21st Century COE project (led by Hayakawa) and the Incubation Business Laboratory Center of Kanazawa University. The electron microscopy studies were partly conducted by a JEOL 6400 at Electron Microscopy Unit of the Australian National University. Frank Brink is thanked for the maintenance of the laboratory. The Durango apatite was kindly provided by Noriko Hasebe. Monika Wilk-Alemany extracted Sr, Nd and CO_2 from the carbonates for mass spectrometric analysis. S.A. thanks Orlando Vaselli for his assistance during the field work, and Kyoko N. Matsukage and Natsue Abe for their assistance in collecting samples. Critical comments from Alberto Zanetti and two anonymous reviewers, and editorial comments from Roberta L. Rudnick significantly improved the manuscript. We are also grateful to V. J. Rajesh and B. B. Payot for the grammatical comments on the manuscript. This study is partly supported by a Grant-in-Aid for Scientific Research of the Ministry of Education, Culture, Sports, Science and Technology of Japan (No. 17740349) to T. M.

Appendix A. Major-element analyses of whole-rock compositions of standard materials distributed from GSJ

In Appendix A, we report whole-rock analyses of selected standard materials (one peridotite JP-1, one gabbro JGb-2, two basalts JB-2 and JB-3, two andesites JA-1 and JA-2, two granites JG-1a and JG-2, and one rhyolite JR-1) determined by XRF at Nagoya University (Table A).

Table A
Analytical values (XRF) and recommended values (Recom.) of GSJ standard rocks

GSJ	JP-1 peridotite		JGb-2 gabbro		JB-2 basalt		JB-3 basalt		JA-1 andesite		JA-2 andesite		JG-1a granite		JG-2 granite		JR-1 rhyolite	
	XRF	Recom.	XRF	Recom.	XRF	Recom.	XRF	Recom.	XRF	Recom.	XRF	Recom.	XRF	Recom.	XRF	Recom.	XRF	Recom.
SiO_2	42.17	42.38	46.93	46.47	52.86	53.25	51.28	50.96	64.12	63.97	56.52	56.42	72.24	72.30	76.78	76.83	75.18	75.45
TiO_2	tr.	0.006*	0.54	0.56	1.17	1.19	1.46	1.44	0.88	0.85	0.69	0.66	0.27	0.25	0.03	0.04	0.11	0.11
Al_2O_3	0.71	0.66	23.63	23.48	14.50	14.64	17.30	17.20	15.17	15.22	15.25	15.41	14.20	14.30	12.53	12.47	12.90	12.83
Fe_2O_3	8.48	8.37	6.58	6.69	14.37	14.25	11.46	11.82	6.91	7.07	6.22	6.21	1.96	2.00	0.99	0.97	0.95	0.89
MnO	0.110	0.099	0.129	0.130	0.202	0.218	0.182	0.177	0.151	0.157	0.103	0.108	0.06	0.06	0.02	0.016	0.098	0.099
MgO	44.66	44.60	6.16	6.18	4.60	4.62	5.16	5.19	1.54	1.57	7.78	7.60	0.68	0.69	0.04	0.04	0.12	0.12
CaO	0.53	0.55	14.18	14.10	9.90	9.82	9.75	9.79	5.62	5.70	6.29	6.29	2.07	2.13	0.71	0.70	0.73	0.67
Na_2O	0.03	0.02	0.95	0.92	1.97	2.04	2.79	2.73	4.06	3.84	2.84	3.11	3.36	3.39	3.59	3.54	4.23	4.02
K_2O	tr.	0.003	0.04	0.06	0.44	0.44	0.80	0.78	0.79	0.77	1.81	1.81	3.99	3.96	4.73	4.71	4.43	4.41
P_2O_5	0.004	0.002*	0.013	0.017	0.098	0.101	0.292	0.294	0.160	0.165	0.149	0.146	0.08	0.08	0.01	0.00	0.018	0.021

Recommended values are from Imai et al. (1995). Numbers with a star (*) are preferable data. tr.=lower than detection limit.

References

Ahijado, A., Casillas, R., Nagy, G., Fernández, C., 2005. Sr-rich minerals in a carbonatite skarn, Fuerteventura, Canary Islands (Spain). Mineral. Petrol. 84, 107–127.

Arai, S., Ishimaru, S., Okrugin, V.M., 2003. Metasomatized harzburgite xenoliths from Avacha volcano as fragments of mantle wedge of the Kamchatka arc: an implication for the metasomatic agent. Isl. Arc. 12, 233–245.

Arai, S., Takada, S., Michibayashi, K., Kida, M., 2004. Petrology of peridotite xenoliths from Iraya volcano, Philippines, and its implication for dynamic mantle-wedge processes. J. Petrol. 45, 369–389.

Bedini, R.M., Bodinier, J.L., 1999. Distribution of incompatible trace elements between the constituents of spinel peridotite xenoliths: ICP-MS data from the East African Rift. Geochim. Cosmochim. Acta 63, 3883–3900.

Bedini, R.M., Bodinier, J.L., Dautria, J.M., Morten, L., 1997. Evolution of LILE-enriched small melt fractions in the lithospheric mantle: a case study from the East African Rift. Earth Planet. Sci. Lett. 153, 67–83.

Belousova, E.A., Griffin, W.L., O'Reilly, S.Y., Fisher, N.I., 2002. Apatite as an indicator mineral for mineral exploration: trace-element compositions and their relationship to host rock type. J. Geochem. Explor. 76, 45–69.

Bodinier, G., Vasseur, G., Vernieres, J., Dupuy, C., Fabries, J., 1990. Mechanisms of mantle metasomatism: geochemical evidence from the Lherz orogenic peridotite. J. Petrol. 31, 597–628.

Bodinier, J.L., Merlet, C., Bedini, R.M., Simien, F., Remaidi, M., Garrido, C.J., 1996. Distribution of niobium, tantalum, and other highly incompatible trace elements in the lithospheric mantle: the spinel paradox. Geochim. Cosmochim. Acta 60, 545–550.

Bodinier, J.L., Menzies, M.A., Shimizu, N., Frey, F.A., McPherson, E., 2004. Silicate, hydrous and carbonate metasomatism at Lherz, France: contemporaneous derivatives of silicate melt–harzburgite reaction. J. Petrol. 45, 299–320.

Boriani, A.C., Villa, I.M., 1997. Geochronology of regional metamorphism in the Ivrea–Verbano Zone and Serie dei Laghi, Italian Alps. Schweiz. Mineral. Petrogr. Mitt. 77, 381–401.

Brassinnes, S., Balaganskaya, E., Demaiffe, D., 2005. Magmatic evolution of the differentiated ultramafic, alkaline and carbonatite intrusion of Vuoriyarvi (Kola Peninsula, Russia). A LA-ICP-MS study of apatite. Lithos 85, 76–92.

Bühn, B., Wall, F., Le Bas, M.J., 2001. Rare-earth element systematics of carbonatitic fluorapatites, and their significance for carbonatite magma evolution. Contrib. Mineral. Petrol. 141, 572–591.

Castellarin, A., Lucchini, F., Rossi, P.L., Selli, L., Simboli, G., Bosellini, A., Sommavilla, E., 1980. Middle Triassic magmatism in southern Alps II: a geodynamic model. Riv. Ital. Paleontol. 85, 1111–1124.

Castellarin, A., Lucchini, F., Rossi, P.L., Selli, L., Simboli, G., 1988. The Middle Triassic magmatic–tectonic arc development in the Southern Alps. Tectonophysics 146, 79–89.

Cawthorn, R.G., 1975. The amphibole peridotite–metagabbro complex, Finero, northern Italy. J. Geol. 83, 437–454.

Chalot-Prat, F., Arnold, M., 1999. Immiscibility between calciocarbonatitic and silicate melts and related wall rock reactions in the upper mantle: a natural case study from Romanian mantle xenoliths. Lithos 46, 627–659.

Coltorti, M., Siena, F., 1984. Mantle tectonite and fractionate peridotite at Finero (Italian Western Alps). N. Jh. Min. Abh. 149, 225–244.

Cumming, G.L., Köppel, V., Ferraio, A., 1987. A lead isotope study of the northeastern Ivrea Zone and the adjoining Ceneri zone (N-Italy): evidence for a contaminated subcontinental mantle. Contrib. Mineral. Petrol. 97, 19–30.

Dautria, J.M., Dupuy, C., Takherist, D., Dostal, J., 1992. Carbonate metasomatism in the lithospheric mantle: peridotite xenoliths from a melilititic district of the Sahara basin. Contrib. Mineral. Petrol. 111, 37–52.

Demény, A., Vennemann, T.W., Hegner, E., Nagy, G., Milton, J.A., Embey-Isztin, A., Homonnay, Z., Dobosi, G., 2004. Trace element and C–O–Sr–Nd isotope evidence for subduction-related carbonate-silicate melts in mantle xenoliths (Pannonian Basin, Hungary). Lithos 75, 89–113.

Doglioni, C., 1987. Tectonics of the Dolomites (Southern Alps, Northern Italy). J. Struct. Geol. 9, 181–193.

Exley, R.A., Smith, J.V., 1982. The role of apatite in mantle enrichment processes and in the petrogenesis of some alkali basalt suites. Geochim. Cosmochim. Acta 46, 1375–1384.

Ferrario, A., Garuti, G., 1990. Platinum-group mineral inclusions in chromitites of the Finero mafic–ultramafic complex (Ivrea-Zone, Italy). Mineral. Petrol. 41, 124–143.

Ferraris, C., Grobety, B., Früh-Green, G.L., Wessicken, R., 2004. Intergrowth of graphite within phlogopite from Finero ultramafic complex (Italian Western Alps): implications for mantle crystallization of primary-texture mica. Eur. J. Mineral. 16, 899–908.

Grieco, G., Ferrario, A., Von Quadt, A., Koeppel, V., Mathez, E.A., 2001. The zircon-bearing chromitites of the phlogopite peridotite of Finero (Ivrea Zone, Southern Alps): evidence and geochronology of a metasomatized mantle slab. J. Petrol. 42, 89–101.

Grieco, G., Ferrario, A., Mathez, E.A., 2004. The effect of metasomatism on the Cr-PGE mineralization in the Finero Complex, Ivrea Zone, Southern Alps. Ore Geol. Rev. 24, 299–314.

Griffin, W.L., O'Reilly, S.Y., Stabel, A., 1988. Mantle metasomatism beneath western Victoria, Australia: II. Isotopic geochemistry of Cr-diopside lherzolite and Al-augite pyroxenites. Geochim. Cosmochim. Acta 52, 449–459.

Handy, M.R., Zingg, A., 1991. The tectonic and rheological evolution of an attenuated cross section of the continental crust: Ivrea crustal section, southern Alps, northwestern Italy and southern Switzerland. Geol. Soc. Amer. Bull. 103, 236–253.

Hartmann, G., Wedepohl, K.H., 1993. The composition of peridotite tectonites from the Ivrea Complex, northern Italy: residues from melt extraction. Geochim. Cosmochim. Acta 57, 1761–1782.

Hauri, E.H., Shimizu, N., Dieu, J.J., Hart, S.R., 1993. Evidence for hotspot-related carbonatite metasomatism in the oceanic upper mantle. Nature 365, 221–227.

Hunziker, J., 1974. Rb–Sr and K–Ar age determination and the Alpine tectonic history of the western Alps. Mem. Ist. Geol. Mineral. Univ. Padova 31, 1–54.

Hunziker, J., Zingg, A., 1982. Zur genese der ultrabasischen gesteine der Ivrea-Zone. Schweiz. Mineral. Petrogr. Mitt. 62, 483–486.

Imai, N., Terashima, H., Itoh, S., Ando, A., 1995. 1994 compilation values for GSJ reference samples, "Igneous rock series". Geochem. J. 29, 91–95.

Ionov, D.A., O'Reilly, S.Y., Genshaft, Y.S., Kopylova, M.G., 1996. Carbonate-bearing mantle peridotite xenoliths from Spitsbergen: phase relationships, mineral compositions and trace-element residence. Contrib. Mineral. Petrol. 125, 375–392.

Ionov, D.A., Bodinier, J.L., Mukasa, S.B., Zanetti, A., 2002. Mechanisms and sources of mantle metasomatism: major and trace element compositions of peridotite xenoliths from Spitsbergen in the context of numerical modeling. J. Petrol. 43, 2219–2259.

Ionov, D.A., Chazot, G., Chauvel, C., Merlet, C., Bodinier, J.L., 2006. Trace element distribution in peridotite xenoliths from Tok, SE Siberian Craton: a record of pervasive, multi-stage metasomatism in shallow refractory mantle. Geochim. Cosmochim. Acta 70, 1231–1260.

Ishida, Y., Morishita, T., Arai, S., Shirasaka, M., 2004. Simultaneous in-situ multi-element analysis of minerals on thin section using LA-ICP-MS. Sci. Rep. Kanazawa Univ. 48, 31–42.

Kaliwoda, M., Altherr, R., Meyer, H.P., 2007. Composition and thermal evolution of the lithospheric mantle beneath the Harrat Uwayrid, eastern flank of the Red Sea rift (Saudi Arabia). Lithos 99, 105–120.

Kaeser, B., Kalt, A., Pettke, T., 2007. Crystallization and breakdown of metasomatic phases in graphite-bearing peridotite xenoliths from Marsabit (Kenya). J. Petrol. 48, 1725–1760.

Keller, J., Hoefs, J., 1995. Stable isotope characteristics of recent natrocarbonatites from Oldoinyo Lengai. In: Bell, K., Keller, J. (Eds.), Carbonatite volcanism. Springer-Verlag, Berlin, pp. 113–123.

Laurora, A., Mazzucchelli, M., Rivalenti, G., Vannucci, R., Zanetti, A., Barbieri, M.A., Cingolani, C.A., 2001. Metasomatism and melting in carbonated peridotite xenoliths from the mantle wedge: the Gobernador Gregores case (southern Patagonia). J. Petrol. 42, 69–87.

Leake, B.E., Woolley, A.R., Arps, C.E.S., Birch, W.D., Gilbert, M.C., Grice, J.D., Hawthorne, F.C., Kato, A., Kisch, H.J., Krivovichev, V.G., Linthout, K., Laird, J., Mandarino, J., Maresch, W.V., Nickel, R.H., Rock, N.M.S., Schumacher, J.C., Smith, D.C., Stephenson, N.C.N., Ungaretti, L., Whittaker, E.J.W., Youzhi, G., 1997. Nomenclature of amphiboles: report of the subcommittee on amphiboles of the International Mineralogical Association, commission on new minerals and mineral names. Am. Mineral. 82, 1019–1037.

Lensch, G., 1968. Die ultramafitite der Zone von Ivrea und ihre geologische intterpretation. Schweiz. Mineral. Petrogr. Mitt. 48, 91–102.

Longerich, H.P., Jackson, S.E., Günther, D., 1996. Laser ablation inductively coupled plasma mass spectrometric transient signal data acquisition and analyte concentration calculation. J. Anal. Atom. Spectr. 11, 899–904.

Lu, M., Hoffmann, A.W., Mazzucchelli, M., Rivalenti, G., 1997. The mafic–ultramafic complex near Finero (Ivrea–Verbano Zone), II. Geochronology and isotope geochemistry. Chem. Geol. 140, 223–235.

Ludwig, K.R., 1998. On the treatment of concordant uranium–lead ages. Geochim. Cosmochim. Acta 62, 665–676.
Matsumoto, T., Morishita, T., Masuda, J., Fujioka, T., Takebe, M., Yamamoto, K., Arai, S., 2005. Noble gases in the Finero Phlogopite–Peridotites, Italian Western Alps. Earth Planet. Sci. Lett. 238, 130–145.
McDonough, W.F., Sun, S.S., 1995. The composition of the Earth. Chem. Geol. 120, 223–253.
McDowell, F.W., McIntosh, W.C., Farley, K.A., 2005. A precise ^{40}Ar–^{39}Ar reference age for the Durango apatite (U–Th)/He and fission-track dating standard. Chem. Geol. 214, 249–263.
McInnes, B.I.A., Cameron, E.M., 1994. Carbonated, alkaline hybridizing melts from a sub-arc environment: mantle wedge samples from the Tabar–Lihir–Tanga–Feni arc, Papua New Guinea. Earth Planet. Sci. Lett. 122, 125–141.
Moine, B.N., Grégoire, M., O'Reilly, Y., Delpech, G., Sheppard, S.M.F., Lorand, J.P., Renac, C., Giret, A., Cottin, J.Y., 2004. Carbonatite melt in oceanic upper mantle beneath the Kerguelen Archipelago. Lithos 75, 239–252.
Morishita, T., Arai, S., Green, D.H., 2003a. Evolution of low-Al orthopyroxene in the Horoman Peridotite, Japan: an unusual indicator of metasomatising fluids. J. Petrol. 44, 1237–1246.
Morishita, T., Arai, S., Tamura, A., 2003b. Petrology of an apatite-rich layer in the Finero Phlogopite–Peridotite massif, Italian Western Alps: implications for evolution of a metasomatizing agent. Lithos 69, 37–49.
Morishita, T., Ishida, Y., Arai, S., 2005a. Simultaneous determination of multiple trace element compositions in thin (< 30 μm) layers of BCR-2G by 193 nm ArF excimer laser ablation-ICP-MS: implications for matrix effect and element fractionation on quantitative analysis. Geochem. J. 39, 327–340.
Morishita, T., Ishida, Y., Arai, S., Shirasaka, M., 2005b. Determination of multiple trace element compositions in thin (< 30 μm) layers of NIST SRM 614 and 616 using laser ablation ICP-MS. Geostand. Geoanal. Res. 29, 107–122.
Navon, O., Stolper, E., 1987. Geochemical consequences of melt percolation: the upper mantle as a chromatographic column. J. Geol. 95, 285–307.
Nicolas, A., Polino, R., Hirn, A., Nicolich, R., ECORS-CROP working group, 1990. ECORS-CROP traverse and deep structure of the western Alps: a synthesis. Mém. Soc. Geol. Fr. 156, 15–27 N.S.
Oppizzi, P., Schaltegger, U., 1999. Zircon-bearing plagioclasites from the Finero complex (Ivrea zone): dating a Late Triassic mantle hic-cup? Schweiz. Mineral. Petrogr. Mitt. 79, 330–331.
O'Reilly, S., Griffin, W.L., 1988. Mantle metasomatism beneath western Victoria, Australia: I. Metasomatic processes in Cr-diopside lherzolites. Geochim. Cosmochim. Acta 52, 433–447.
O'Reilly, S., Griffin, W.L., 2000. Apatite in the mantle: implications for metasomatic processes and high heat production in Phanerozoic mantle. Lithos 53, 217–232.
Ottolini, L., Le Fèvre, B., Vannucci, R., 2004. Direct assessment of mantle boron and lithium contents and distribution by SIMS analyses of peridotite minerals. Earth Planet. Sci. Lett. 228, 19–36.
Pearce, N.J.G., Perkins, W.T., Westgate, J.A., Gorton, M.P., Jackson, S.E., Neal, C.R., Chenery, S.P., 1997. A compilation of new and published major and trace element data for NIST SRM 610 and NIST SRM 612 glass reference materials. Geostand. Newsl. 21, 114–144.
Peressini, G., Quick, J.E., Sinigoi, S., Hofmann, A.W., Fanning, M., 2007. Duration of a large mafic intrusion and heart transfer in the lower crust: a SHRIMP U–Pb zircon study in the Ivrea–Verbano Zone (Western Alps, Italy). J. Petrol. 48, 1185–1218.
Philippot, P., Selverstone, J., 1991. Trace-element rich brines in eclogitic veins: implications for fluid compositions and transport during subduction. Contrib. Mineral. Petrol. 106, 417–430.
Philippot, P., Agrinier, P., Scambelluri, M., 1998. Chlorine cycling during subduction of altered oceanic crust. Earth Planet. Sci. Lett. 161, 33–44.
Pisa, G., Castellarin, A., Lucchini, F., Rossi, P.L., Simboli, G., Bosellini, A., Sommavilla, E., 1980. Middle Triassic magmatism in Southern Alps I: a review of the general data in the Dolomites. Riv. Ital. Paleontol. 85, 1093–1110.
Prouteau, G., Scaillet, B., Pichavant, M., Maury, R., 2001. Evidence for mantle metasomatism by hydrous silicic melts derived from subducted oceanic crust. Nature 410, 197–200.
Raffone, N., Fèvre, B.L., Ottolini, L., Vannucchi, R., Zanetti, A., 2006. Light-lithophile element metasomatism of Finero peridotite (W Alps): a secondary-ion mass spectrometry study. Microchim. Act 155, 251–255.
Rivalenti, G., Zanetti, A., Mazzucchelli, M., Vannucci, R., Cingolani, C., 2004. Equivocal carbonatite markers in the mantle xenoliths of the Patagonia backarc: the Gobernador Gregores case (Santa Cruz Province, Argentina). Contrib. Mineral. Petrol. 147, 647–670.
Rosatelli, G., Wall, F., Stoppa, F., 2007. Calcio-carbonatite melts and metasomatism in the mantle beneath Mt. Vulture (Southern Italy). Lithos 99, 229–248.
Rubatto, D., 2002. Zircon trace element geochemistry: partitioning with garnet and the link between U–Pb ages and metamorphism. Chem. Geol. 184, 123–138.
Rudnick, R.L., McDonough, W.F., Chappell, B.W., 1993. Carbonatite metasomatism in the northern Tanzanian mantle: petrographic and geochemical characteristics. Earth Planet. Sci. Lett. 114, 463–475.
Rudnick, R.L., McDnough, W.F., Orpin, A., 1994. Northern Tanzanian peridotite xenoliths: a comparison with Kaapvaal peridotites and inferences on metasomatic interactions. In: Meyer, H.O.A., Leonardos, O. (Eds.), Kimberlites, Related Rocks and Mantle Xenoliths, Vol. 1 (Proceedings Fifth International Kimberlite Conference). C.P.R.M., Brasilia, pp. 336–353.
Sano, Y., Oyama, T., Terada, K., Hidaka, H., 1999a. Ion microprobe U–Pb dating of apatite. Chem. Geol. 153, 249–258.
Sano, Y., Terada, K., Hidaka, H., Yokoyama, K., Nutman, A.P., 1999b. Palaeoproterozoic thermal events recorded in the ~4.0 Ga Acasta gneiss, Canada: evidence from SHRIMP U–Pb dating of apatite and zircon. Geochim. Cosmochim. Acta 63, 899–905.
Sano, Y., Terada, K., Takeno, S., Taylor, L.A., McSween Jr., H.Y., 2000. Ion microprobe uranium–thorium–lead dating of Shergotty phosphates. Meteor. Planet. Sci. 35, 341–346.
Scambelluri, M., Piccardo, G.B., Philippot, P., Robbiano, A., Negretti, L., 1997. High salinity fluid inclusions formed from recycled seawater in deeply subducted alpine serpentinite. Earth Planet. Sci. Lett. 148, 485–499.
Seifert, W., Kämpf, H., Wasternack, J., 2000. Compositional variation in apatite, phlogopite and other accessory minerals of the ultramafic Delitzsch complex, Germany: implication for cooling history of carbonatites. Lithos 53, 81–100.
Siena, F., Coltorti, M., 1989. The peterogenesis of a hydrated mafic–ultramafic complex and the role of amphibole fractionation at Finero (Italian Western Alps). N. Jb. Miner. Mh. 6, 255–274.
Stähle, V., Frenzel, G., Kober, B., Michard, A., Puchelt, H., Schneider, W., 1990. Zircon syenite pegmatites in the Finero peridotite (Ivrea zone): evidence for a syenite from a mantle source. Earth Planet. Sci. Lett. 101, 196–205.
Stähle, V., Frenzel, G., Hess, J.C., Saupé, F., Schmidt, S.T., Schneider, W., 2001. Permian metabasalt and Triassic alkaline dykes in the northern Ivrea zone: clues to the post-Variscan geodynamic evolution of the Southern Alps. Schweiz. Mineral. Petrogr. Mitt. 81, 1–21.
Sugisaki, R., Shimomura, T., Ando, K., 1977. An automatic X-ray fluorescence method for the analysis of silicate rocks. J. Geol. Soc. Japan 83, 725–733 (in Japanese with English abstract).
Takayanagi, Y., Yamamoto, K., Yogo, S., Adachi, M., 2000. Depositional environment of the Cretaceous Shimanto bedded cherts from the Fukura area, Kochi Prefecture, inferred from major element, rare earth element and normal paraffin compositions. J. Geol. Soc. Japan 106, 632–645.
Takazawa, E., Okayasu, T., Satoh, K., 2003. Geochemistry and origin of the basal lherzolites from the northern Oman ophiolite (northern Fizh block). Geochem. Geophys. Geosys. 4. doi:10.1029/2001GC000232.
Takebe, M., Yamamoto, K., 2003. Geochemical fractionation between porcellanite and host sediment. J. Geol. 111, 301–312.
Tiepolo, M., Bottazzi, P., Foley, S.F., Oberti, R., Vannucci, R., Zanetti, A., 2001. Fractionation of Nb and Ta from Zr and Hf at mantle depths: the role of titanian pargasite and kaersutite. J. Petrol., 42, 221–232.
Tsuboi, M., 2005. The use of apatite as a record of initial $^{87}Sr/^{86}Sr$ ratios and indicator of magma processes in the Inagawa pluton, Ryoke belt, Japan. Chem. Geol. 221, 157–169.
Vannucci, R., Piccardo, G.B., Rivalenti, G., Zanetti, A., Rampone, E., Ottolini, L., Oberti, R., Mazzucchelli, M., Bottazzi, P., 1995. Origin of LREE-depleted amphiboles in the subcontinental mantle. Geochim. Cosmochim. Acta 59, 1763–1771.
Vannucci, R., Bottazzi, P., Wulff-Pedersen, E., Neumann, E.R., 1998. Partitioning of REE, Y, Sr, Zr and Ti between clinopyroxene and silicate melts in the mantle under La Palma (Canary Islands): implications for the nature of the metasomatic agents. Earth Planet. Sci. Lett. 158, 39–51.
Vavra, G., Schmid, R., Gebauer, D., 1999. Internal morphology, habit and U–Th–Pb microanalysis of amphibolite-to-granulite facies zircons: geochronology of the Ivrea Zone (Southern Alps). Contrib. Mineral. Petrol. 134, 380–404.
Voshage, H., Hunziker, J.C., Hofmann, A.W., Zingg, A., 1987. A Nd and Sr isotopic study of the Ivrea zone, Southern Alps, N-Italy. Contrib. Mineral. Petrol. 97, 31–42.
Von Quadt, A., Ferrario, A., Diella, V., Hansmann, W., Vavra, G., Köppel, V., 1993. U–Pb ages of zircons from chromitites of the phlogopite perdotite of Finero, Ivrea zone, N-Italy. Schweiz. Mineral. Petrogr. Mitt. 73, 137–138.
Watson, E.B., 1980. Apatite and phosphorus in mantle source regions: an experimental study of apatite/melt equilibria at pressure to 25 kbar. Earth Planet. Sci. Lett. 51, 322–335.
Wendt, I., 1989. Geometric considerations of the three-dimensional U/Pb data presentation. Earth Planet. Sci. Lett. 94, 231–235.
Wulff-Pedersen, E., Neumann, E.R., Vannucci, R., Bottazzi, P., Ottolini, L., 1999. Silicic melts produced by reaction between peridotite and infiltrating basaltic melts: ion probe data on glasses and minerals in veined xenoliths from La Palma Canary Islands. Contrib. Mineral. Petrol. 137, 59–82.
Yamamoto, K., Morishita, T., 1997. Preparation of standard composites for the trace element analysis by X-ray fluorescence. J. Geol. Soc. Japan 103, 1037–1045 (in Japanese with English abstract).
Yamamoto, K., Yamashita, F., Adachi, M., 2005. Precise determination of REE for sedimentary reference rocks issued by the Geological Survey of Japan. Geochem. J. 39, 289–297.
Yaxley, G.M., Kamenetsky, V., 1999. In situ origin for glass in mantle xenoliths from southeastern Australia: insights from trace element compositions of glasses and metasomatic phases. Earth Planet. Sci. Lett. 172, 97–109.
Yaxley, G.M., Crawford, A.J., Green, D.H., 1991. Evidence for carbonatite metasomatism in spinel peridotite xenoliths from western Victoria, Australia. Earth Planet. Sci. Lett. 107, 305–317.
Yaxley, G.M., Green, D.H., Kamenetsky, V., 1998. Carbonatite metasomatism in the Southeastern Australian Lithosphere. J. Petrol. 39, 1917–1930.
York, D., 1969. Least squares fitting of a straight line with correlated errors. Earth Planet. Sci. Lett. 5, 320–324.
Zaccarini, F., Stumpfl, E.F., Garuti, G., 2004. Zirconolite and Zr–Th–U minerals in chromitites of the Finero complex, Western Alps, Italy: evidence for carbonatite-type metasomatism in a subcontinental mantle plume. Can. Mineral. 42, 1825–1845.
Zanetti, A., Mazzucchelli, M., Rivalenti, G., Vannucci, R., 1999. The Finero phlogopite–peridotite massif: an example of subduction-related metasomatism. Contrib. Mineral. Petrol. 134, 107–122.
Zanetti, A., Vannucci, R., Bottazi, P., Oberti, R., Ottolini, L., 1996. Infiltration metasomatism at Lherz as monitored by systematic ion-microprobe investigations close to a hornblendite vein. Chem. Geol. 134, 113–133.
Zindler, A., Hart, S., 1986. Chemical geodynamics. Ann. Rev. Earth Planet. Sci. 14, 493–571.
Zinngrebe, E., Foley, S.F., 1995. Metasomatism in mantle xenoliths from Gees, West Eiffel, Germany: evidence for the genesis of calc-alkaline glasses and metasomatic Ca-enrichment. Contrib. Mineral. Petrol. 122, 79–96.